JAOCR

Official Journal of the American Osteopathic College of Radiology

NEURORADIOLOGY

Guest Editor: Benjamin O. Cornwell, D.O.

Editor-in-Chief: Daniel J. Wale, D.O.

April 2021, Vol. 10, Issue 2

JAOCR

Official Journal of the American Osteopathic College of Radiology

Aims and Scope

The Journal of the American Osteopathic College of Radiology (JAOCR) is designed to provide practical up-to-date reviews of critical topics in radiology for practicing radiologists and radiology trainees. Each quarterly issue covers a particular radiology subspecialty and is composed of high-quality review articles and case reports that highlight differential diagnoses and important teaching points.

Access to Articles

All articles published in the JAOCR are open access online. Subscriptions to the journal are not required to view or download articles. Reprints are not available.

Copyrights

Materials published in the JAOCR are protected by copyright. No part of this publication may be reproduced without written permission from the AOCR.

Guide for Authors

Submissions for the JAOCR are by invitation only. If you were invited to submit an article and have questions regarding the content or format, please contact the appropriate Guest Editor for that particular issue. Although contributions are invited, they are subject to peer review and final acceptance.

JAOCR

NEURORADIOLOGY

Guest Editor: Benjamin O. Cornwell, D.O.

From the Editor

Review Articles

Differential-Based Case Reviews

JAOCR at the Viewbox

In this Issue

Benjamin O. Cornwell, D.O.

Assistant Professor of Radiology, University of Oklahoma College of Medicine
Neuroradiology Section Chief, Department of Radiological Sciences, University of Oklahoma Health Sciences Center

"Life will knock us down, but we can choose whether or not to stand back up."
—Jackie Chan

I would like to thank Dr. Wale and the JAOCR for giving me the opportunity to serve as a guest editor for this neuroradiology issue. It has been my privilege to work alongside my colleagues at the University of Oklahoma on this project. I also would like to thank the authors for their time and hard work.

This issue addresses several topics in neuroradiology with the general radiologist in mind. The first review article, by Dr. Borden, covers surface anatomy of the brain in detail. Accurate localization is paramount, and this article provides the tools to correctly place pathology. This review can also be used as a quick reference during a busy workday.

I wrote the second review article "Absence of the Normal Posterior Pituitary Bright Spot in Children." This article discusses the posterior pituitary gland and the pathologic processes that cause the normal bright signal within the gland to disappear. These cases can be challenging because it is not uncommon for the lesion to be very small. On occasion, the only imaging feature initially detected is absence of the normal posterior pituitary bright spot.

The case review by Dr. Choudhry, "Cystic Lesion of the Mandibular Ramus," tackles the challenging topic of odontogenic lesions. The review presents a framework on how to approach cystic odontogenic lesions. The case review by Dr. Memon and Mr. Khan, "Rare Developmental Brainstem Abnormality," discusses several developmental posterior fossa abnormalities. Many of these disorders may go undiagnosed prior to imaging.

Two interesting JAOCR at the Viewbox cases wrap up the issue. Dr. Lal presents a recently described rare pediatric brain tumor: polymorphous low-grade neuroepithelial tumor of the young (PLNTY). Dr. Alhyari shows a case of subpial hemorrhage in a newborn, which is a rare type of hemorrhage primarily seen in young children.

I hope you enjoy this issue and find it beneficial in your day-to-day practice. I personally have learned a great deal while preparing this manuscript.

A Patterned Approach to Cerebral Gyri and Sulci for the General Radiologist

Neil M. Borden, M.D.

Department of Radiological Sciences, University of Oklahoma College of Medicine, Oklahoma City, OK
*Figures 3A, 4, 5, 6, 7, 8, 16 and 18 are reprinted with permission from Alastair J.E. Moore, MD, medical illustrator.

Evaluation of CT and MRI studies of the brain in routine clinical practice not only requires an accurate identification and description of abnormal findings, but precise localization is essential as well. Localization is not only critical for the neurosurgeon/neurologist but having this knowledge and being cognizant of the functional deficits related to a specific anatomic location allows the interpreting radiologist to focus attention on specific regions of the brain. This pictorial review will provide the basic tools a radiologist needs to generate an accurate and precise description of neurologic-based diseases by providing a pattern recognition approach and will focus on gyral and sulcal anatomy. The MRI and CT images in this pattern approach will be supplemented with high-resolution, computer-generated 3-D images.

Variability in gyral/sulcal anatomy is the rule, as no two individuals have the exact same pattern. There are also certain normal asymmetries of the cerebral hemispheres that one will often encounter. Despite this, there is a general schema (pattern) from which the interpreter can call upon to adapt to unexpected individual variances that may not look exactly like the textbook picture. The typical patterns of surface anatomy will be presented along with functional attributes when pertinent.
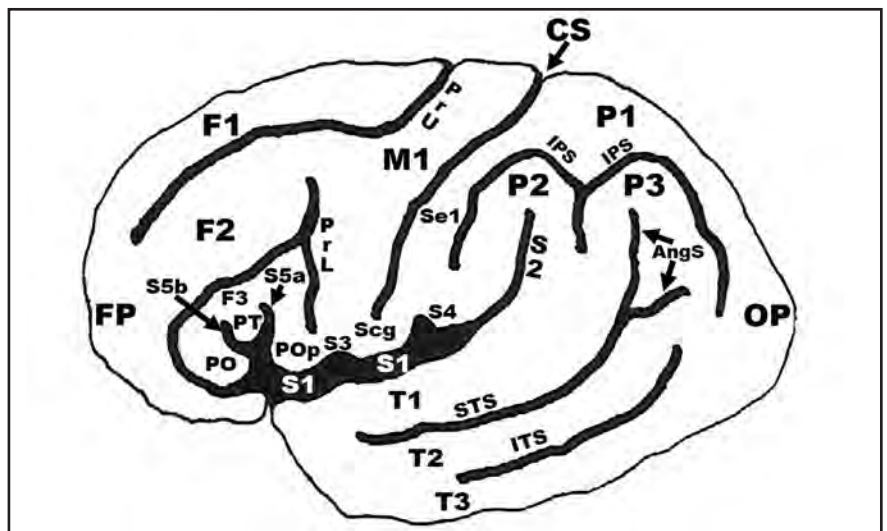

FIGURE 1. *Lateral graphic illustrating the typical pattern of the major gyri and sulci along the lateral convexity of the brain. (See Figure Legend Key at end of article.)*

Basic Concepts of Cerebral Anatomy

The traditional concept has been that the brain consisted of 4 lobes: the frontal, temporal, parietal, and occipital lobes. Current concepts and nomenclature have expanded the number of lobes to 6, which now includes the insular and limbic lobes.[1] The limbic lobe/system refers to a functional unit of the brain involved with emotions and instinctual behaviors.

General Considerations

The frontal, parietal, temporal, occipital and insular lobes surround the sylvian fissure (lateral sulcus) along the lateral convexity in an anterior to posterior orientation. The sylvian fissure has various branches including the anterior horizontal and anterior ascending ramus, the anterior and posterior subcentral sulci, and the posterior ascending ramus. A small posterior descending ramus is often present (**Figure 1**). A common normal hemispheric asymmetry involving the sylvian fissure exists. In a significant portion of individuals, the posterior ascending ramus of the sylvian fissure on the right has a steeper, more vertical orientation than on the left (**Figures 2A, 2B**). The midline interhemispheric fissure separates one cerebral hemisphere
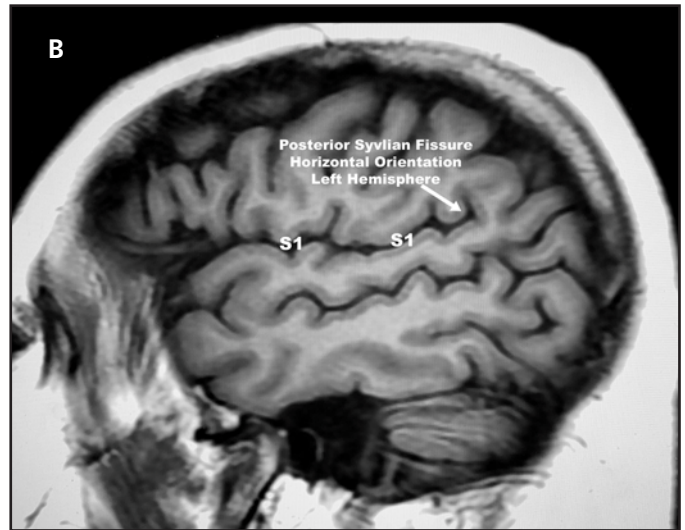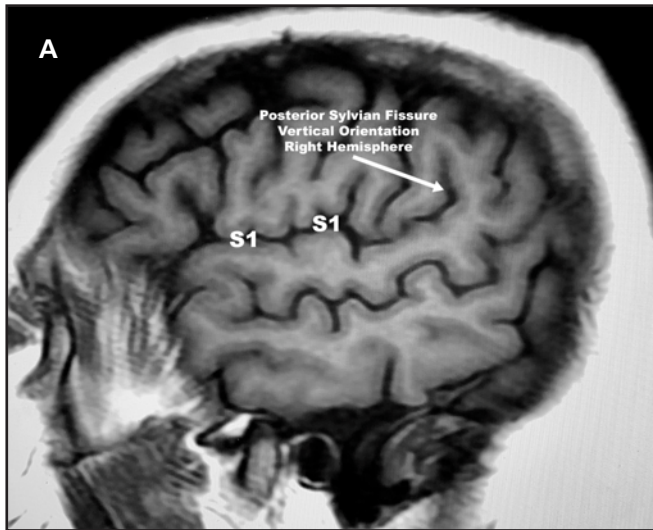
FIGURE 2A. *Sagittal T1-weighted MR image of the right cerebral hemisphere illustrating the more vertical orientation of the posterior ascending ramus of the sylvian fissure.*

FIGURE 2B. *Sagittal T1-weighted MR image of the left cerebral hemisphere illustrating the more horizontal orientation of the posterior ascending ramus of the sylvian fissure.*
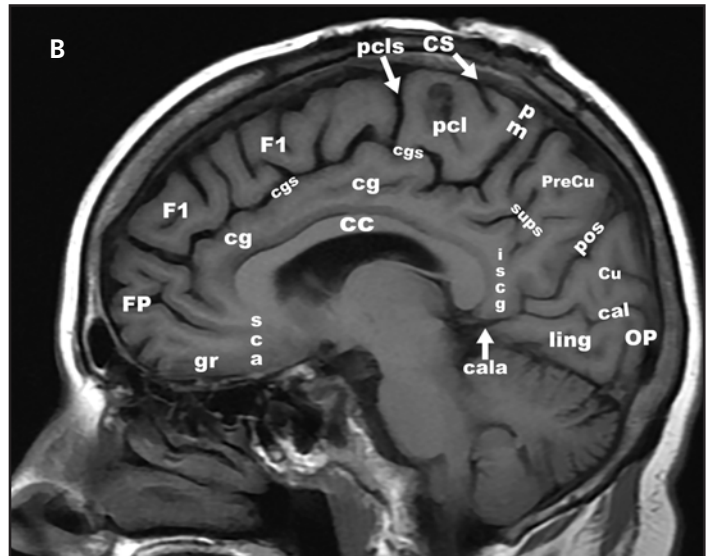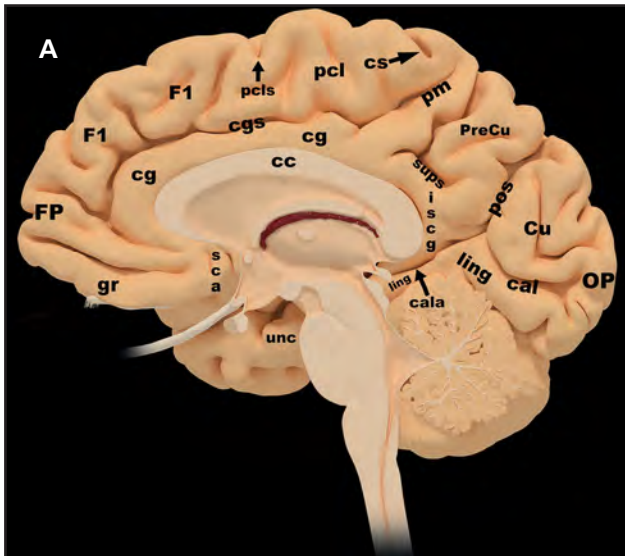

FIGURE 3A. *A 3D midsagittal view illustrating the typical pattern of cerebral gyri and sulci.*

FIGURE 3B. *Midsagittal T1-weighted MR image of the brain illustrating the typical pattern of cerebral gyri and sulci.*

from the other. The basal portion of the anterior frontal lobes sits atop the orbital plates of the frontal bones in the anterior cranial fossa. The temporal lobes sit upon the floor of the middle cranial fossa and the occipital lobes lie atop the tentorium cerebelli above the posterior cranial fossa.

Typical Patterns of Cerebral Gyri and Sulci
Typical Pattern – Frontal Lobe
The largest lobe is the frontal lobe extending from the frontal pole to the central sulcus and inferiorly bordered by the cingulate gyrus (part of limbic lobe) along its medial surface (**Figure 3A, 3B**). Over the lateral convexity surface are 3 main gyri oriented longitudinally: superior, middle, and inferior frontal gyri (**Figures 1, 4-10**). The superior frontal gyrus is separated from the middle frontal gyrus by the superior frontal sulcus, which extends posteriorly to dead end or end in a "T" at the superior precentral sulcus. The middle frontal gyrus is the largest frontal gyrus and is separated from the inferior fron-

tal gyrus by the inferior frontal sulcus. Sometimes the middle frontal gyrus is subdivided into superior and inferior sections by an inconstant middle frontal sulcus. An interruption of the pre-central sulcus at the level of the middle frontal gyrus allows the middle frontal gyrus to merge with the anterior margin of the pre-central gyrus. The smallest frontal gyrus and most unusual in shape is the inferior frontal gyrus. It has a triangular or "M" shape and is divided into an anterior pars orbitalis, a middle pars triangularis and a posterior pars **opercularis**
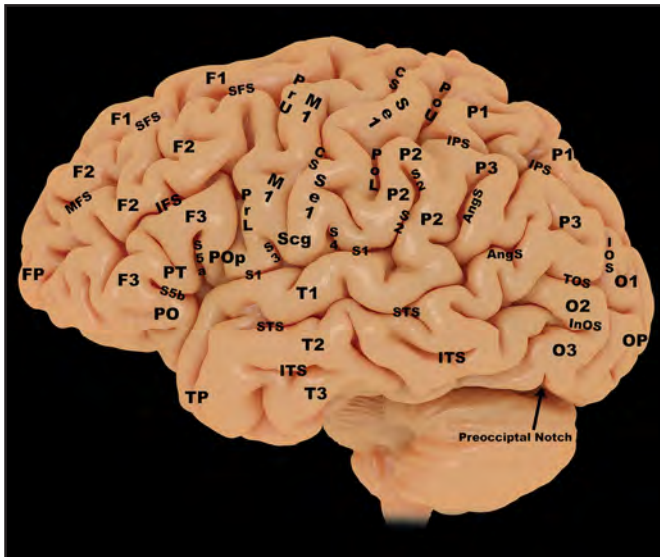
FIGURE 4. *A 3D lateral view illustrating the typical pattern of cerebral gyri and sulci.*

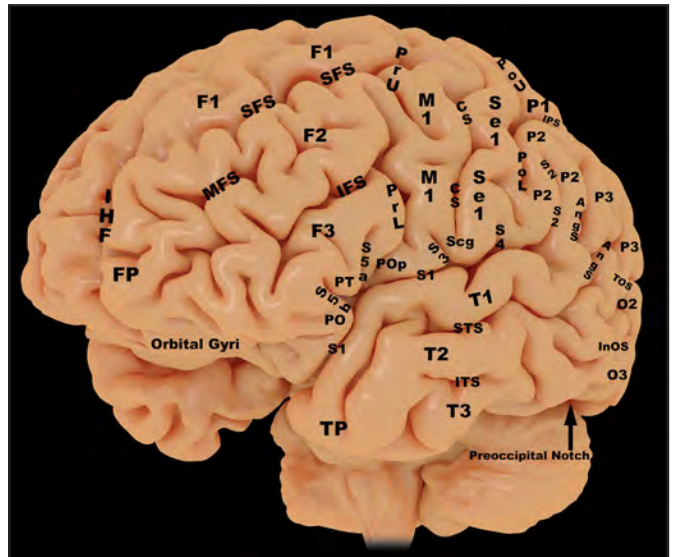**FIGURE 5.** *A 3D anterior oblique view illustrating the typical pattern of the cerebral gyri and sulci.*
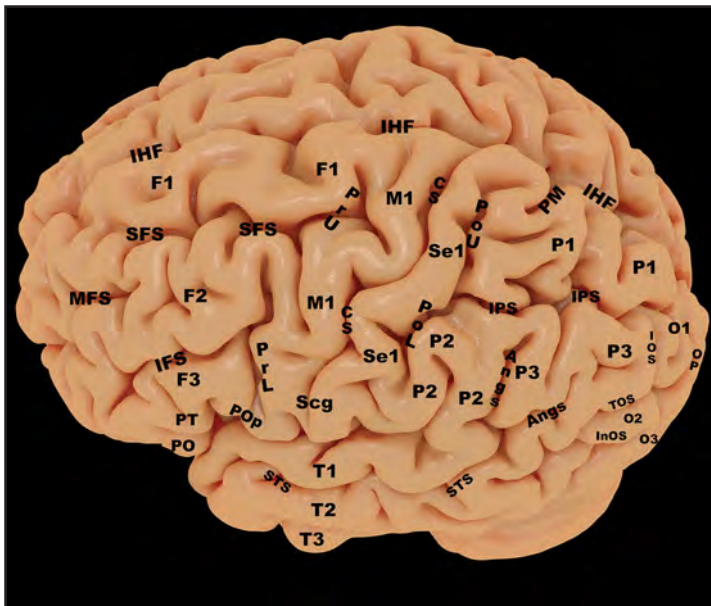
FIGURE 6. *A 3D superior oblique view illustrating the typical pattern of the cerebral gyri and sulci.*
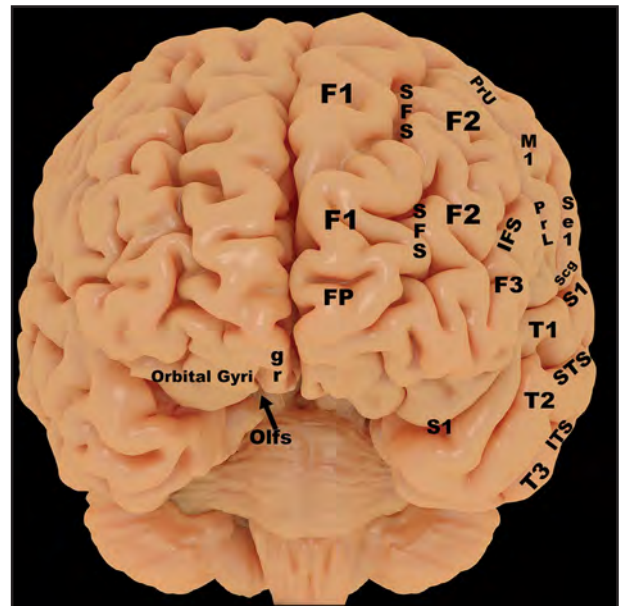
FIGURE 7. *A 3D anterior view illustrating the typical pattern of the cerebral gyri and sulci.*

(**Figure 11**). Pars triangularis and pars opercularis in the language dominant hemisphere (usually the left) correspond to the classical Broca's region[2] responsible for the motor production of language. Injury to the same regions in the language nondominant hemisphere results in disorders of **production of prosody** (the intonation/inflections/ rhythm of speech) providing meaning to spoken language.[3] The anterior horizontal ramus of the sylvian fissure separates pars orbitalis from pars triangularis while the anterior ascending ramus of the sylvian fissure separates pars triangularis from pars opercularis. The inferior frontal gyrus is separated posteriorly from the pre-central gyrus by the inferior pre-central sulcus. Along the lateral convexity surface, the central sulcus (posterior margin of the frontal lobe) extends obliquely from posterior-superior to anterior-inferior, never reaching the sylvian fissure along its inferior margin. Instead, its inferior aspect is surrounded by the "U"-shaped subcentral gyrus (primary gustatory cortex). A characteristic morphology of the pre- and postcentral gyri on parasagittal images allows identification of the primary motor and somatosensory gyri and the central sulcus. This morphologic appearance can be reproduced by interlocking one's hands with the fingers and thumb curled in a "C"-shape with the curled left fingers below the
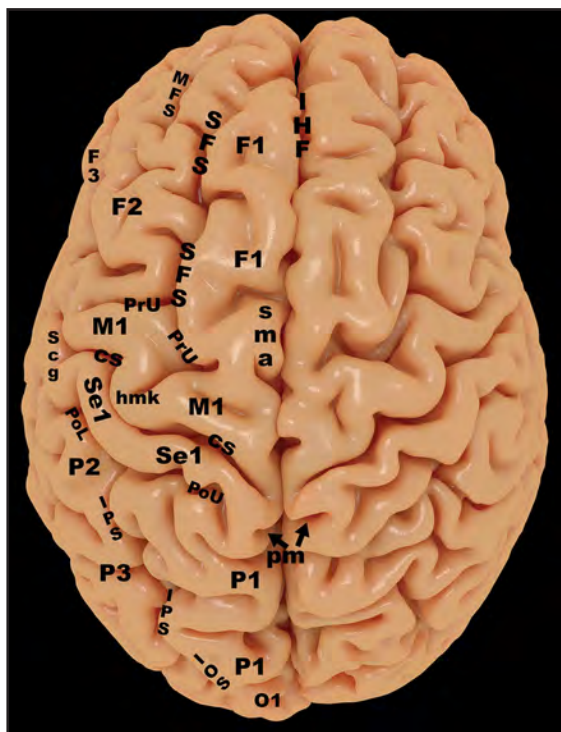
FIGURE 8. *A 3D superior view illustrating the typical pattern of the cerebral gyri and sulci.*
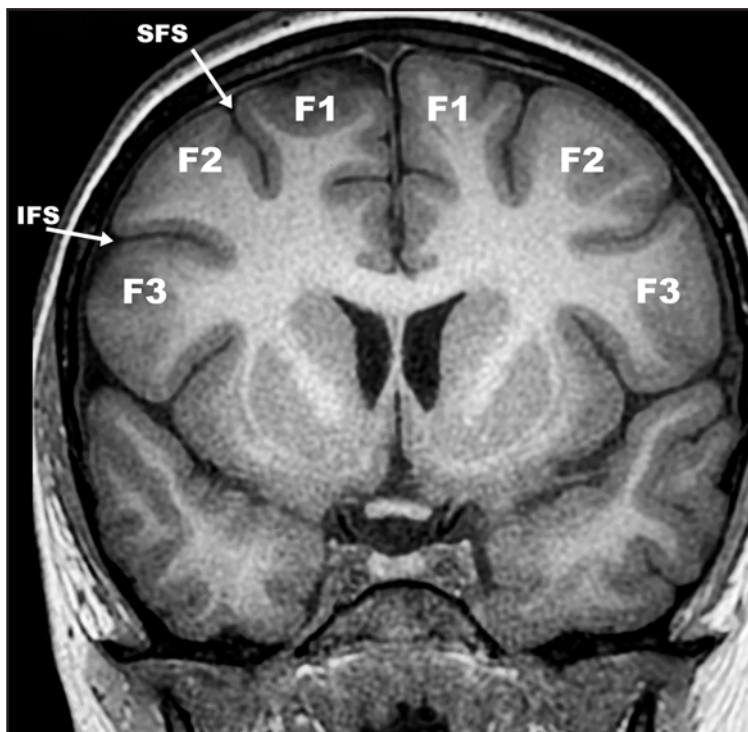
FIGURE 9. *Coronal T1-weighted MR image illustrating the typical pattern of the major frontal gyri and sulci.*

FIGURE 10. *Coronal CT image illustrating the typical pattern of the major frontal gyri and sulci.*
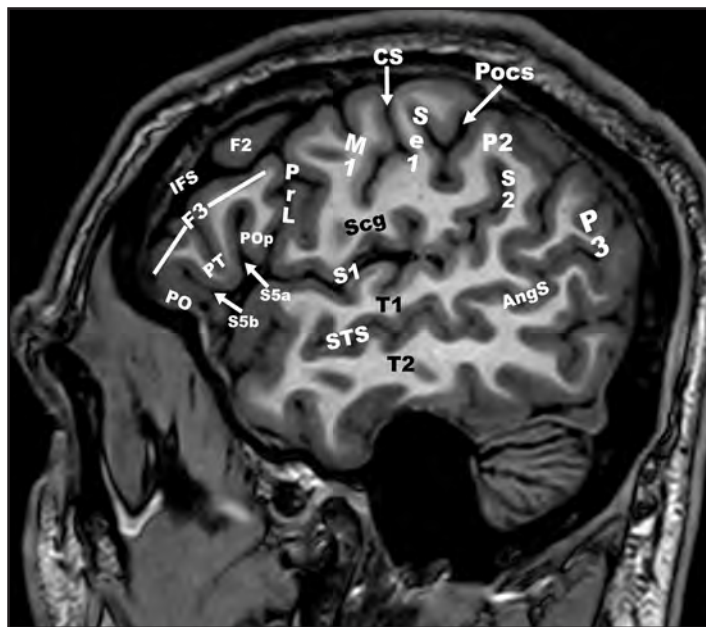
FIGURE 11. *Sagittal T1-weighted MR image illustrating the typical pattern of the major gyri and sulci along the lateral convexity of the brain.*

curled right fingers and the left thumb under the right thumb (**Figures 12A, 12B**). The posteriorly projecting prominence of the pre-central gyrus represents the hand motor knob (motor function for the contralateral hand). The pre-central gyrus (primary motor strip) is thicker/larger than the postcentral gyrus (primary sensory strip). In the axial imaging plane, the hand motor knob region of the pre-central gyrus can be identified by its characteristic upside-down omega shape. Along the medial/interhemispheric aspect of the frontal lobe, the superior/medial frontal gyrus lies above the cingulate sulcus. The posterior aspect of the cingulate sulcus swings upward in a vertical direction and at the vertex splits the medial end of the postcentral gyrus into a bifid configuration. This upward, vertical segment is
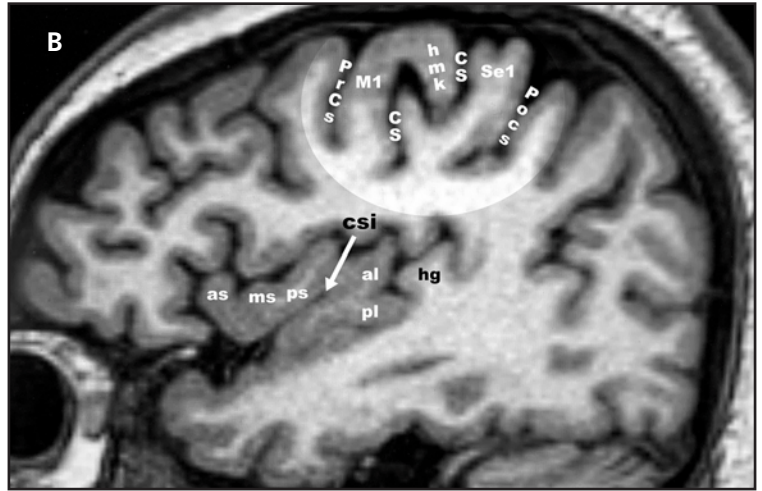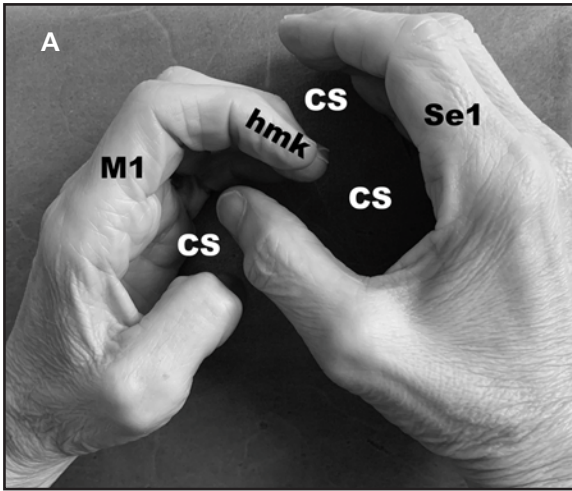
FIGURE 12A. Replication of the sagittal morphology of the pre- (M1) and postcentral (Se1) gyri, surrounding the central sulcus (CS) by interlocking hands and fingers. Note the hand motor knob (hmk) projecting posteriorly from the pre-central gyrus (M1).

FIGURE 12B. Sagittal T1-weighted MR image illustrating the typical pattern of the pre (M1) and postcentral (Se1) gyri, surrounding the central sulcus (CS) and the pre- (PrCs) and postcentral sulci (Pocs). Note the hand motor knob (hmk) projecting posteriorly from the pre-central gyrus (M1). These structures are highlighted with greater brightness. Also illustrated is the insular lobe and adjacent Heschl's gyrus (hg).
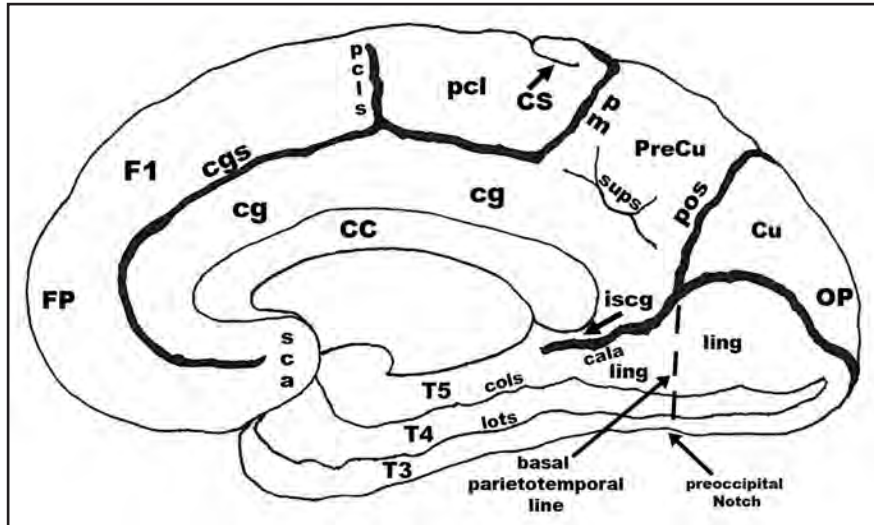
FIGURE 13. Midsagittal graphic illustrating the typical pattern of cerebral gyri and sulci. Also note the imaginary basal parietotemporal line and preoccipital notch.

called pars marginalis or the posterior ascending ramus of the cingulate sulcus. The central sulcus along the lateral convexity reaches the superomedial surface of the hemisphere and curves posteriorly, a few millimeters anterior to and pointing toward pars marginalis (**Figures 3A, 3B, 13**). A variably inconstant vertically oriented paracentral sulcus, which can arise from and project superiorly from the posterior cingulate sulcus or extend inferiorly from the vertex or both, marks the anterior margin of the paracentral lobule, the posterior margin being pars marginalis

and the inferior border being the posterior cingulate sulcus. The superior end of the paracentral sulcus is at the level of, or just anterior to, the superior end of the precentral sulcus. The cingulate gyrus represents the inferior extent of the paracentral lobule (**Figure 3A, 3B, 13**). Along the posterior medial aspect of the superior frontal gyrus, just anterior to the pre-central gyrus in the paracentral lobule near the level of the pre-central sulcus lies the supplementary motor area (SMA) (**Figures 8, 14A, 14B**). This region is functionally involved in the planning and execution

of complex movements of the extremities including the correction of posture during motor activation.[4] SMA activation results in bilateral (but contralateral greater than ipsilateral) effects. Injury to the SMA results in the SMA syndrome characterized by contralateral weakness and speech arrest with near complete recovery in weeks to months. This has important clinical implications for patients undergoing surgery in this region. The basal surface of the frontal lobes sitting above the floor of the anterior cranial fossa consists of a series of orbital gyri (orbitofrontal gyri). The gyrus rectus (straight gyrus) is the most constant of these gyri and is located just above the cribriform plates on each side of the midline. The olfactory sulci lie along the lateral aspect of the gyri recti and lie superior to the olfactory bulbs and tracts. Lateral to the olfactory sulci are the orbital gyri, which are arranged around an "H"-shaped pattern of sulci ("H"-shaped sulcus of Rolando) (**Figure 15, 16**).[5-7] These include the anterior, posterior, medial and lateral orbital gyri. The posteromedial orbital lobule is where the posterior and medial orbital gyri converge.

Typical Pattern – Parietal Lobe
    The parietal lobe consists of the postcentral gyrus and the superior and

FIGURE 14A. Axial CT image through the cerebral hemispheres illustrating the typical pattern of the cerebral gyri and sulci.
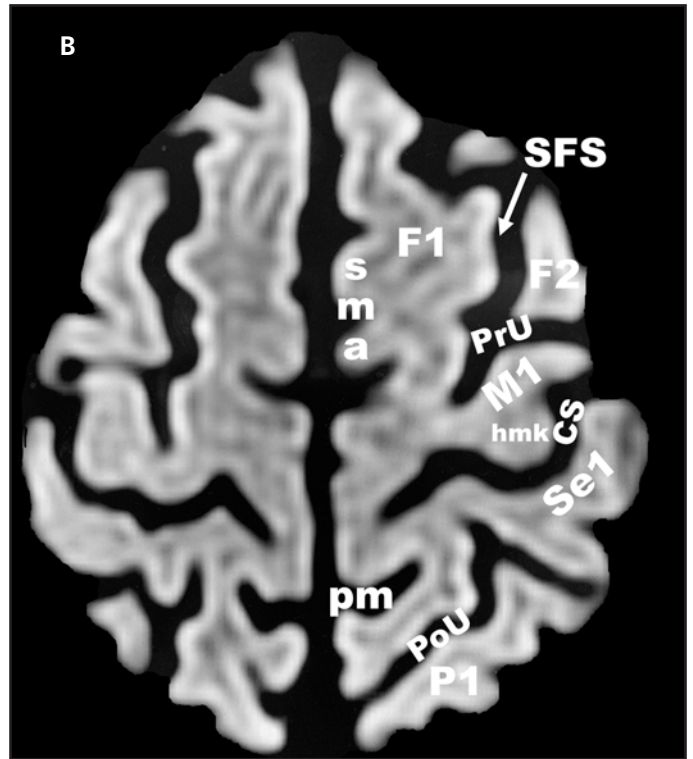
FIGURE 14B. Axial diffusion-weighted trace image through the cerebral hemispheres illustrating the typical pattern of the cerebral gyri and sulci.

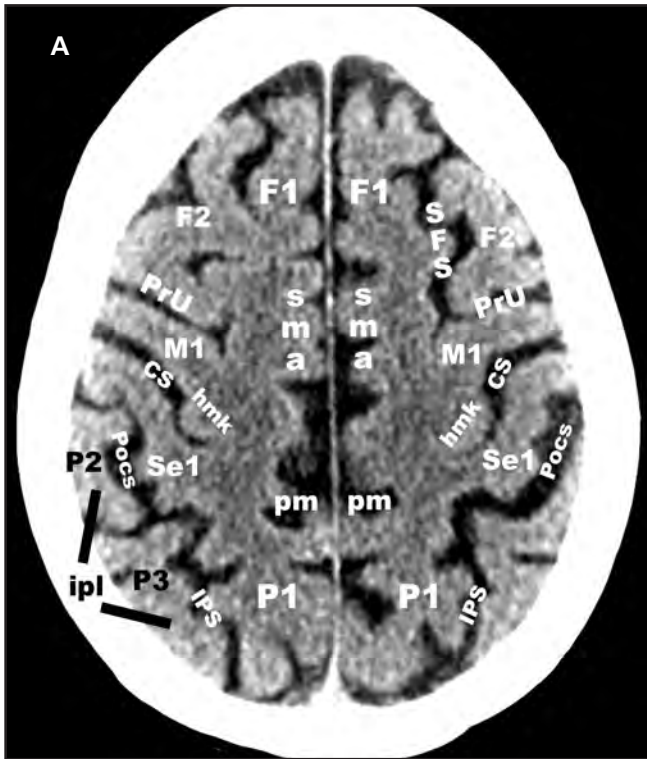**FIGURE 15.** Axial T2-weighted MR image showing the typical pattern of the orbitofrontal gyri surrounding the "H"-shaped sulcus of Rolando.
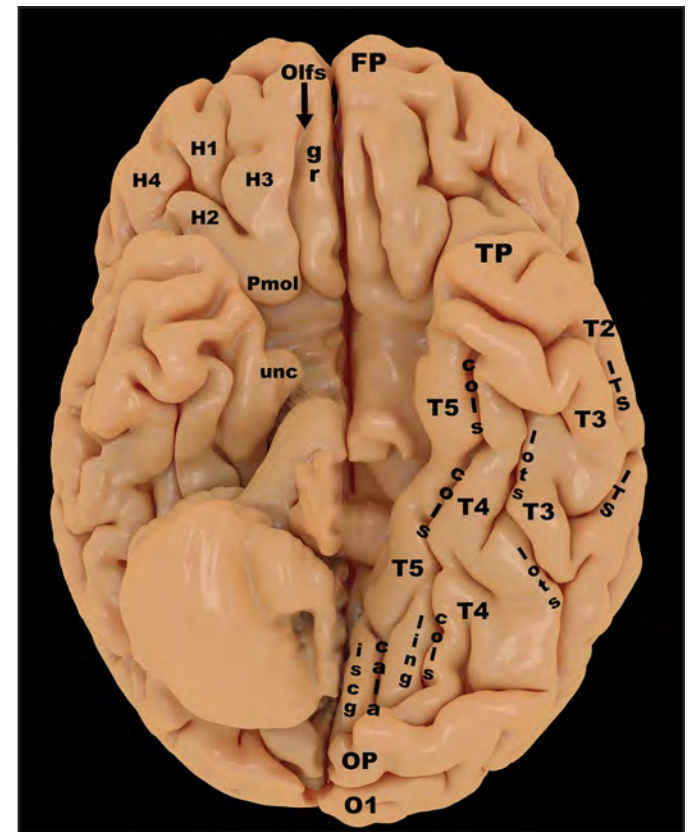
FIGURE 16. A 3D inferior view illustrating the typical pattern of the orbitofrontal gyri and sulci, and temporal and occipital gyri and sulci.
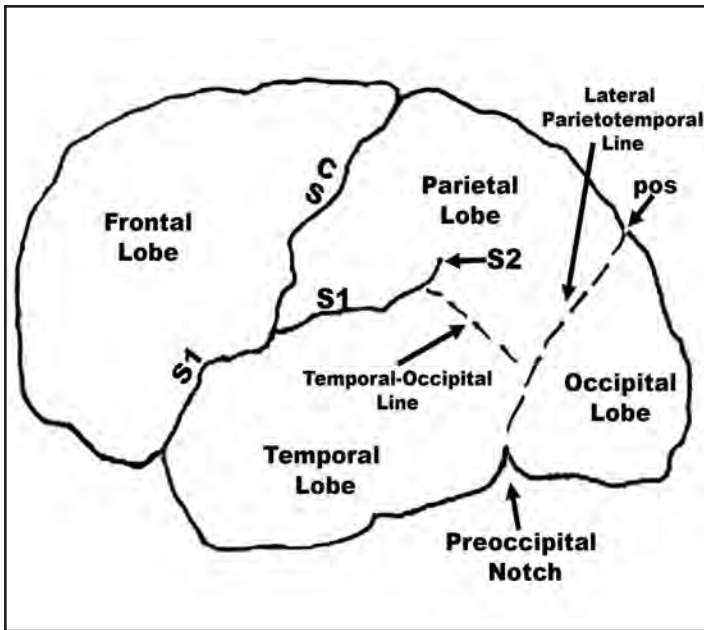
FIGURE 17. *Lateral graphic illustrating the typical pattern of the lobar boundaries including the imaginary lateral parietotemporal and temporal-occipital lines and the preoccipital notch.*
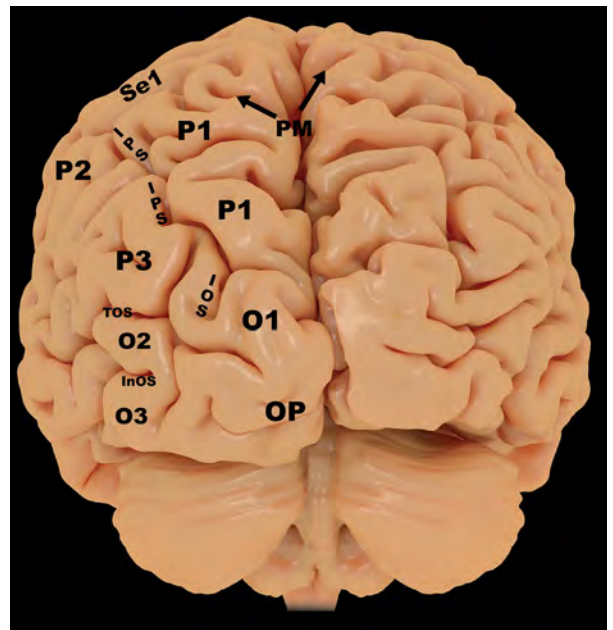
FIGURE 18. *A 3D posterior view illustrating the typical pattern of cerebral gyri and sulci.*
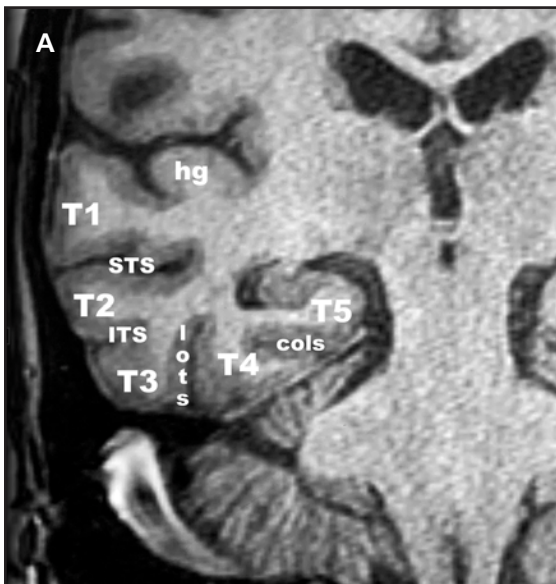
FIGURE 19A. *Coronal T1-weighted MR image illustrating the typical pattern of temporal lobe gyri and sulci and Heschl's gyrus (hg) along the flat superior plane of the temporal lobe.*
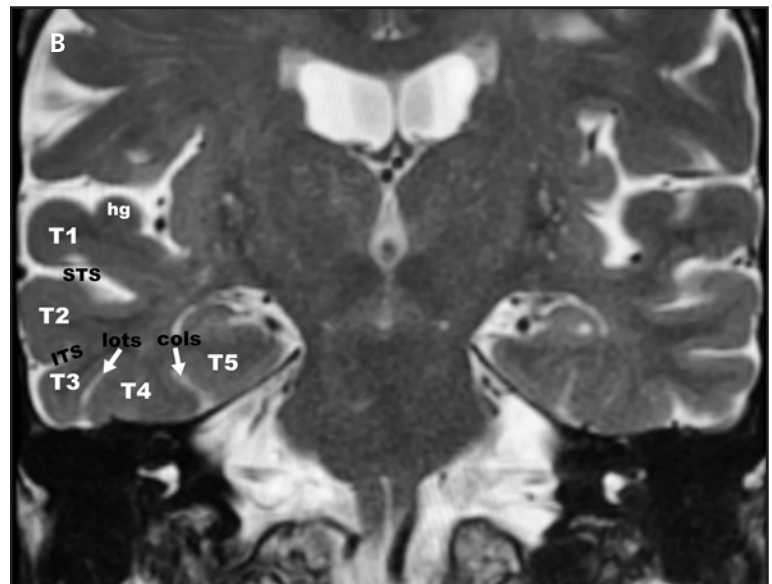
FIGURE 19B. *Coronal T2-weighted MR image illustrating the typical pattern of temporal lobe gyri and sulci and Heschl's gyrus (hg) along the flat superior plane of the temporal lobe.*

inferior parietal lobules (**Figures 1, 4-6, 8, 11**). The superior parietal lobule is located superomedial to the inferior parietal lobule. It extends posteriorly from the postcentral gyrus to the parieto-occipital sulcus along the medial, interhemispheric aspect and is separated from the inferior parietal lobule by the intraparietal sulcus more laterally. The mesial surface of the superior parietal lobule is the precuneus (between the parieto-occipital sulcus and pars marginalis). The precuneus is separated from the cingulate gyrus of the limbic lobe by the subparietal sulcus (**Figures 3A, 3B, 13**). The intraparietal sulcus is obliquely oriented in the anterior to posterior direction (**Figure 1, 4, 6, 14A**). The inferior parietal lobule consists of the supramarginal and angular gyri. The supramarginal gyrus surrounds the posterior ascending ramus of the sylvian fissure. Posterior to the supramarginal gyrus lies the angular gyrus (**Figures 1, 4, 11**). There is a clear demarcation of the parietal lobe from the occipital lobe along the interhemispheric region by the parieto-occipital sulcus, which runs obliquely from anterior-inferior to posterior-superior (**Figures 3A, 3B, 13**). However, along the lateral
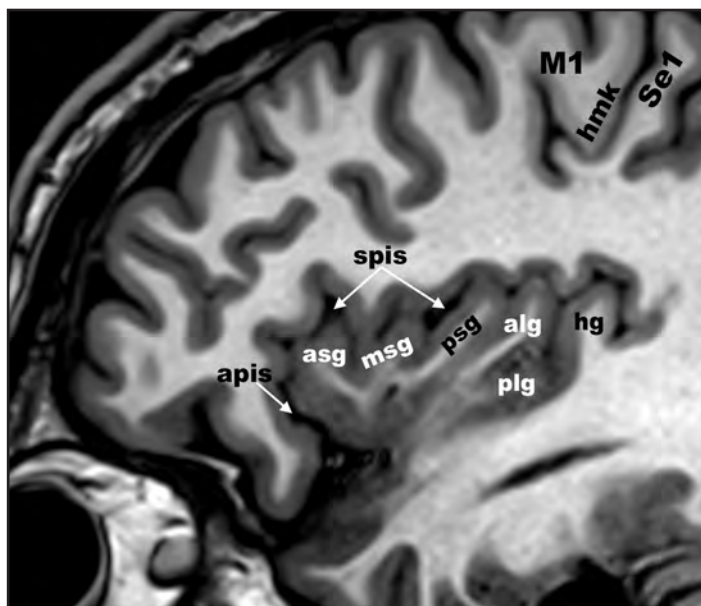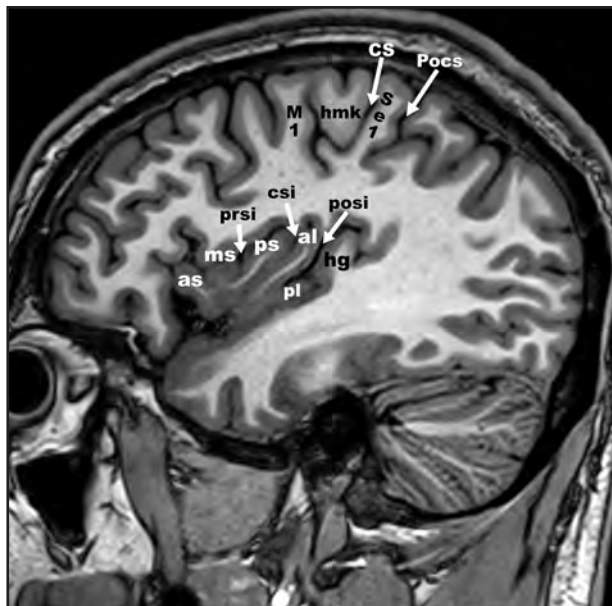
FIGURE 20A. *Sagittal T1-weighted MR image showing the typical pattern of the insular lobe gyri and sulci and the adjacent Heschl's gyrus (hg). Also note the typical morphologic pattern of the pre-(M1), postcentral (Se1) gyri and surrounding sulci.*

FIGURE 20B. *Small field of view sagittal T1-weighted MR image illustrating the typical pattern of the insular lobe gyri and sulci and the adjacent Heschl's gyrus (hg).*

convexity no clear demarcation exists between the parietal and occipital lobes and a commonly used imaginary line to delineate this boundary is the lateral parietotemporal line (created by connecting a line from the preoccipital notch along the lateral undersurface of the cerebral hemisphere) to the point at which the parieto-occipital sulcus reaches the superomedial convexity surface (**Figure 17**). This lateral parietotemporal line also provides a demarcation between the posterior temporal lobe and the occipital lobe. There is also no clear demarcation between the parietal lobe and the temporal lobe over the lateral convexity. Another imaginary line used to delineate this demarcation is the temporo-occipital line, which is drawn from the posterior sylvian fissure to the midpoint along the lateral parietotemporal line (**Figure 17**).[8]

Typical Pattern – Occipital Lobe

The occipital lobe has the most inconstant arrangement of sulci and gyri, and inconsistent descriptions in the literature of its surface pattern creating confusion in delineating its morphologic anatomy. The occipital lobe can be divided into superior, middle and inferior occipital gyri converging posteriorly at the occipital pole (**Figures 4, 18**). When the intraparietal sulcus extends inferiorly along its posterior aspect into the occipital lobe, it is referred to as the intra-occipital sulcus.[5] The superior occipital gyrus (oriented vertically) is located closest to the interhemispheric fissure lying medial to the intra-occipital sulcus and posterior-inferior to the superior parietal lobule with the middle occipital gyrus lateral to the intra-occipital sulcus. The middle and inferior occipital gyri are arranged longitudinally along the posterolateral surface of the hemisphere, paralleling the inferior surface of the hemisphere and separated by a less well-defined inferior occipital sulcus, which is often seen as the posterior extension of the inferior temporal sulcus. The inferior occipital gyrus can be seen as a posterior continuation of the inferior temporal gyrus. The middle occipital gyrus is often the largest occipital gyrus and may be subdivided into superior and inferior portions by an inconstant lateral or middle occipital sulcus.[9] It lies posterior to the junction between the temporal and parietal lobes. The transverse occipital sulcus separates the parietal lobe from the middle occipital gyrus.[10] Along the basal surface of the cerebral hemisphere, an imaginary line (basal parieto-temporal line) drawn from the inferior parieto-occipital sulcus to the preoccipital notch demarcates the temporal from the occipital lobes (**Figure 13**).

Typical Pattern – Temporal Lobe

The temporal lobe lies inferior to the sylvian fissure. It extends posteriorly from the temporal pole in the anterior middle cranial fossa. There is no clear anatomic structure delineating the posterior borders of the temporal lobe from the parietal and occipital lobes. As discussed above, imaginary lateral parietotemporal, temporo-occipital and the basal parietotemporal lines (**Figures 13, 17**) provide direction in locating these posterior boundaries. The lateral convexity of the temporal lobe consists of the superior, middle and inferior temporal gyri and are separated by the superior and inferior temporal sulci (**Figures 1, 4, 19A, 19B**). The superior temporal sulcus has also been named the parallel sulcus since it runs parallel to the sylvian fissure. The posterior aspect of the superior temporal sulcus can be single or bifid and is called the angular sulcus since it leads to the angular gyrus. The flat

superior surface of the temporal lobe is called the superior temporal plane.[9] The transverse temporal gyrus (Heschl's gyrus – primary auditory cortex) extends along the superior temporal plane from posteromedial to anterolateral (**Figures 19A, 19B, and 20A, 20B**). The posterior peri-sylvian area corresponding to Wernicke's area (receptive language) is not a highly localized region[11] and includes the posterior aspect of the superior temporal gyrus and the adjacent supramarginal and angular gyri (inferior parietal lobule).[8] The undersurface (basal surface) of the temporal lobe also consists of three gyri. From medial to lateral, these are the parahippocampal gyrus, the lateral occipitotemporal gyrus (fusiform gyrus) and the inferior temporal gyrus (**Figure 13, 19A, 19B**). The fusiform gyrus is implicated in the function of facial recognition with inability to recognize familiar faces (prosopagnosia) occurring with bilateral or unilateral lesions to the fusiform gyrus.[12] The collateral sulcus separates the parahippocampal gyrus from the lateral occipitotemporal gyrus (fusiform gyrus) and the lateral occipitotemporal sulcus separates the lateral occipitotemporal gyrus (fusiform gyrus) from the inferior temporal gyrus. The inferior temporal gyrus shares the lateral undersurface and inferolateral margins of the temporal lobe. The posterior aspect of the parahippocampal gyrus is continuous with the isthmus of the cingulate gyrus (curving around the splenium of the corpus callosum) (**Figure 13**). Along the basal surface of the temporal lobe, the posterior aspect of the lateral occipitotemporal gyrus (fusiform gyrus) diverges laterally where the medial occipitotemporal gyrus (anterior aspect of the lingual gyrus of the occipital lobe) intercalates itself for a short distance between the more medial parahippocampal/isthmus of cingulate gyrus and the divergent lateral occipitotemporal gyrus. The collateral sulcus maintains its position medial to the lateral occipitotemporal gyrus posteriorly

while the anterior calcarine sulcus separates the medial occipitotemporal gyrus (lingual gyrus) from the parahippocampal/isthmus of the cingulate gyrus (**Figure 13, 16**).

Typical Pattern – Insular Lobe

The insular lobe (**Figures 12B, 20A, 20B**) is identified on gross inspection of the brain by separating the operculum (lips) of the frontal, parietal and temporal lobes. When this is performed, one is looking at the insular cortex consisting of a larger anterior lobule and a smaller posterior lobule separated by the central sulcus of the insula. Most commonly, the anterior lobule consists of 3 short gyri with well-formed anterior and posterior short gyri and a less well-formed middle short gyrus. The precentral sulcus of the insula is located between the middle and posterior short gyri. The smaller posterior lobule of the insula most often consists of an anterior long and posterior long gyrus separated by the postcentral sulcus of the insula. The posterior long gyrus is oriented parallel to the superior temporal plane and lies subjacent to Heschel's gyrus (transverse temporal gyrus). The circular sulcus (anterior, superior and inferior peri-insular sulcus) surrounds the insular lobe.

Typical Pattern – Limbic Lobe/Limbic System

The limbic lobe/system lies along the medial surface of the hemisphere and includes the subcallosal area, the olfactory cortex, the "C"-shaped cingulate gyrus (that follows the contour of the corpus callosum) and parahippocampal gyri (with associated hippocampus and amygdala), connected by the isthmus of the cingulate gyrus that wraps around the splenium of the corpus callosum (**Figures 3A, 3b, 13**). Its boundaries include the cingulate sulcus, the subparietal sulcus and the collateral sulcus. There is an overlap in that the parahippocampal gyrus is included in descriptions as part of both the temporal and limbic lobes.

Conclusion

Feeling comfortable with gyral and sulcal anatomy (surface anatomy) of the brain is challenging but critically important when interpreting cross-sectional imaging studies. Acquisition of this knowledge is best accomplished through a routine and repetitive practice of reviewing this information from case to case, which over time will become assimilated and reflexive. Knowledge of the typical patterns will allow you to problem solve when encountering atypical patterns of surface anatomy. You will find a sense of confidence in the ability to localize lesions, which will be appreciated by your neurology and neurosurgical colleagues who rely on your interpretive skills.

REFERENCES

1. Borden NM, Forseen SE. Supertentorial Compartment: Cerebral Hemispheres. In: Imaging Anatomy of the Human Brain: A Comprehensive Atlas Including Adjacent Structures. demosMedical; 2015:464.
2. Afifi AK, Bergman RA. Functional Neuroanatomy: Text and Atlas. 2nd ed. McGraw HIll Professional; 2005.
3. Patel S, Oishi K, Wright A, et al. Right hemisphere regions critical for expression of emotion through prosody. Front Neurol 2018;9(APR). doi:10.3389/fneur.2018.00224
4. Naidich TP, Hof PR, Yousry TA, Yousry I. The motor cortex: anatomic substrates of function. Neuroimaging Clin N Am 2001;11(2):171-193, vii-viii. Accessed June 21, 2020. http://www.ncbi.nlm.nih.gov/pubmed/11489733
5. Ribas GC. The cerebral sulci and gyri. Neurosurg Focus 2010;28(2). doi:10.3171/2009.11.FOCUS09245
6. Tamaraz J, Comair Y. Atlas of Regional Anatomy of the Brain Using MRI. Springer-Verlag Berlin Heidelberg; 2000. doi:10.1007/3-540-30672-2
7. Naidich T, Castillo M, Cha S, Smirniotopoulos J. Inferior Surface: Frontal Lobes. In: Imaging of the Brain. Elsevier; 2012:139.
8. Naidich TP, Hof PR, Gannon PJ, Yousry TA, Yousry I. Anatomic substrates of language: emphasizing speech. Neuroimaging Clin N Am 2001;11(2):305-341, ix.
9. Naidich T, Castillo M, Cha S, Smirniotopoulos J. Anatomy: Lateral Surface: Occipital Lobe. In: Imaging of the Brain. Elsevier; 2012:131.
10. Naidich T, Castillo M, Cha S, Smirniotopoulos J. Figure 9-6. In: Imaging of the Brain. Elsevier; 2012:132.
11. Binder JR. The Wernicke area. Neurology 2015;85(24):2170-2175. doi:10.1212/WNL.0000000000002219
12. Corrow SL, Dalrymple KA, Barton JJS. Prosopagnosia: current perspectives. Eye Brain 2016;8:165-175. doi:10.2147/EB.S92838

Figure Legend Key

Frontal Lobe Gyri
F1 – Superior Frontal Gyrus
F2 = Middle Frontal Gyrus
F3 = Inferior Frontal Gyrus
PO = Pars Orbitalis
PT = Pars Triangularis
POp = Pars Opercularis
H1 = Anterior Orbital Gyrus
H2 = Posterior Orbital Gyrus
H3 = Medial Orbital Gyrus
H4 = Lateral Orbital Gyrus
Pmol = Posteromedial Orbital Lobule
gr = Gyrus Rectus
M1 = Pre-Central Gyrus (Primary Motor Strip)

Frontal Lobe Sulci
SFS = Superior Frontal Sulcus
MFS = Middle Frontal Sulcus
IFS = Inferior Frontal Sulcus
Olfs = Olfactory Sulcus
HR = "H"-Shaped Sulcus of Rolando
PrU = Upper Pre-Central Sulcus
PrL = Lower Pre-Central Sulcus
PrCs = Pre-Central Sulcus

Temporal Lobe Gyri
T1 = Superior Temporal Gyrus
T2 = Middle Temporal Gyrus
T3 = Inferior Temporal Gyrus
T4 = Lateral Occipital Temporal Gyrus (Fusiform Gyrus)
T5 = Parahippocampal Gyrus
unc = Uncus of Temporal Lobe

Temporal Lobe Sulci
STS = Superior Temporal Sulcus (Parallel Sulcus)
AngS = Angular Sulcus
ITS = Inferior Temporal Sulcus
lots = Lateral Occipital Temporal Sulcus
cols = Collateral Sulcus
hg = Heschl's (Transverse Temporal) Gyrus

Parietal Lobe Gyri
Se1 = Postcentral Gyrus (Primary Somatosensory Strip)
P1 = Superior Parietal Lobule
P2 = Supramarginal Gyrus
P3 = Angular Gyrus
ipl = Inferior Parietal Lobule

Parietal Lobe Sulci
pm = Pars Marginalis (Ascending Ramus of Cingulate Sulcus)
Pocs = Postcentral Sulcus
PoU = Upper Postcentral Sulcus
PoL = Lower Postcentral Sulcus
IPS = Intra-Parietal Sulcus
sups = Subparietal Sulcus

Occipital Lobe Gyri
O1 = Superior Occipital Gyrus
O2 = Middle Occipital Gyrus
O3 = Inferior Occipital Gyrus
Cu = Cuneus
ling = Lingual Gyrus (Medial Occipital-Temporal Gyrus)

Occipital Lobe Sulci
IOS = Intra-Occipital Sulcus (Superior Occipital Sulcus)
LOS = Lateral (Middle) Occipital Sulcus
TOS = Transverse Occipital Sulcus
InOS = Inferior Occipital Sulcus
pos = Parieto-Occipital Sulcus
cal = Calcarine Sulcus
cala = Anterior Calcarine Sulcus

Insular Lobe Gyri
ali = Anterior Lobule of Insula
as = Anterior Short Gyrus
ms = Middle Short Gyrus
ps = Posterior Short Gyrus
pli = Posterior Lobule of Insula
al = Anterior Long Gyrus
pl = Posterior Long Gyrus
prgi = Pre-Central Gyrus of Insula
pogi = Postcentral Gyrus of Insula

Insular Lobe Sulci
csi = Central Sulcus of Insula
prsi = Pre-Central Sulcus of Insula
posi = Postcentral Sulcus of Insula
apis = Anterior Peri-insular Sulcus (Circular Sulcus) of insula
spis = Superior Peri-Insular Sulcus (Circular Sulcus) of Insula
ipis = Inferior Peri-Insular Sulcus (Circular Sulcus) of Insula

Limbic Lobe Gyri
cg = Cingulate Gyrus
iscg = Isthmus of Cingulate Gyrus
T5 = Parahippocampal Gyrus
sca = Subcallosal Area

Sylvian Fissure (Lateral Fissure)
S1 = Sylvian fissure
S2 = Posterior ascending ramus of sylvian fissure
S3 = Anterior subcentral sulcus
S4 = Posterior subcentral sulcus
S5a = Anterior ascending ramus
S5b = Anterior horizontal ramus

Miscellaneous
cc = Corpus callosum
cgs = Cingulate sulcus
CS = Central sulcus (Rolandic Fissure)
FP = Frontal pole
IHF = Interhemispheric fissure
OP = Occipital pole
pcl = Paracentral lobule
pcls = Paracentral sulcus
PreCu = Precuneus
Scg = Subcentral Gyrus
sma = Supplementary motor area
TP = Temporal pole

Absence of the Normal Posterior Pituitary Bright Spot in Children

Benjamin O. Cornwell, D.O.

Department of Radiological Sciences, University of Oklahoma College of Medicine, Oklahoma City, OK

Central diabetes insipidus is a common indication for MR imaging of the pituitary hypothalamic axis in children. The clinical presentation often includes polyuria, polydipsia, and nocturia related to impaired secretion of antidiuretic hormone. Imaging will generally demonstrate absence of a normal posterior bright spot, and there may be an associated abnormality involving the pituitary infundibulum and/or hypothalamus. The underlying etiology can be idiopathic, post-traumatic, postsurgical, congenital, neoplastic, autoimmune, infectious, or inflammatory. Understanding the normal pituitary anatomy and MRI appearance as well as the characteristic imaging findings of many common causes of central diabetes insipidus is paramount.

Anatomy and Physiology of the Pituitary Gland

The pituitary gland has two distinct origins. The anterior gland (adenohypophysis) arises from Rathke's pouch on the roof of the foregut. The posterior pituitary (neurohypophysis) and median eminence of the hypothalamus arise from neuroectoderm in the floor of the forebrain.[1] The infundibulum arises from the ventromedial hypothalamus and is a variably hollow tube containing cerebrospinal fluid (CSF) referred to as the infundibular recess of the third ventricle. The pars intermedia is between the adenohypophysis and neurohypophysis. The pars tuberalis extends from the hypothalamus along the infundibulum before entering the adenohypophysis (**Figure 1**).

The anterior pituitary gland is larger than the posterior lobe and makes up two-thirds of the total pituitary volume. The anterior pituitary gland consists of 5 separate cell types each of which secrete different hormones. The anterior pituitary hormones include adrenocorticotropic hormone (ACTH), growth hormone (GH), follicle-stimulating hormone (FSH) and luteinizing hormone (LH), prolactin (PRL), and thyrotropin-stimulating hormone (TSH). Discussion of these individual hormones is beyond the scope of this article.

The posterior lobe of the pituitary gland consists of pituicytes, tanycytes, and the terminal portion of axons whose cell bodies are within the hypothalamus. Paraventricular and supraoptic nuclei within the hypothalamus produce vasopressin and oxytocin. These posterior pituitary hormones are then transported from the hypothalamus through the infundibulum into the posterior lobe of the pituitary gland. These neurosecretory granules (neurophysins) are thought to contain proteins that produce the hyperintense intrinsic T1 signal within the posterior lobe of the pituitary gland.[2,3] Vasopressin, also known as antidiuretic hormone (ADH), is a nonapeptide that is important in maintaining osmoregulation, cardiovascular control, and homeostasis. The most important stimuli that evoke vasopressin release are increased plasma osmolality, decreased arterial pressure, and reduced cardiac filling. Oxytocin stimulates milk ejection from the breast in response to suckling and stimulates uterine contraction during labor to deliver the fetus and placenta.[4]

Normal Development of the Pituitary Gland on MRI

In the fetus and neonate, the anterior lobe of the pituitary gland has a convex superior margin and hyperintense T1 signal in relation to the cortex or gray matter (**Figure 2**). The size of the anterior lobe and hyperintense T1 signal within the anterior lobe will slowly diminish until two months after birth. At two months, the anterior pituitary will assume the appearance expected in a child. That is, the
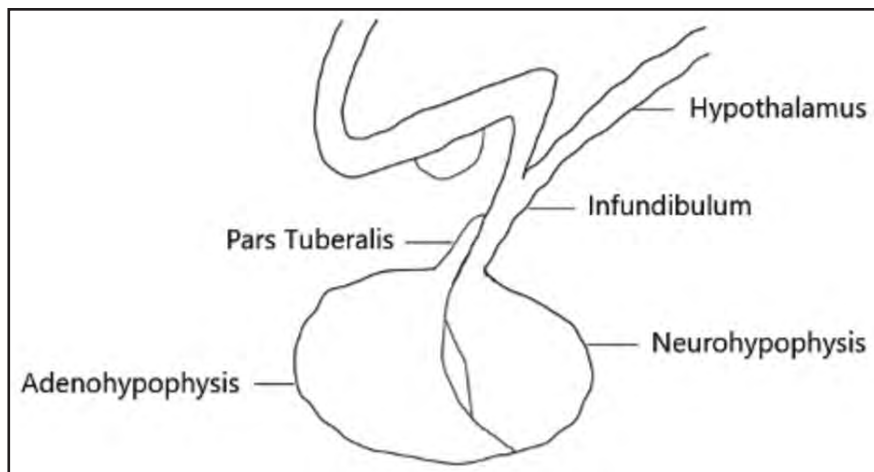
FIGURE 1. *Illustration of the normal pituitary gland.*

FIGURE 2. *Sagittal T1 image demonstrating the normal appearance of the pituitary in a 5-day-old infant. Note the bright adenohypophysis.*

anterior lobe will have a flat or slightly concave superior margin and T1 signal intensity similar to gray matter (**Figure 3**).

The posterior pituitary gland has hyperintense T1 signal in relation to the brain at birth and this will continue into adulthood. The normal posterior pituitary bright spot should measure 1.2 to 8.5 mm in the long axis and 0.4 to 4.4 mm in the short axis. All neonates and children should have a posterior pituitary bright spot; absence is always abnormal. Up to 48% of normal adults will have absence of the posterior pituitary bright spot.[5,6] Why the posterior bright spot is not visualized in all normal adults remains unknown. One theory is that the amount of ADH stored in the posterior pituitary decreases with age, leading to a gradual decrease in size and then disappearance of the bright spot in some normal adult patients.[5,6]

The normal pituitary infundibulum should smoothly taper from superior to inferior. The AP and transverse diameters of the normal pituitary infundibulum are 2.32 +/- 0.39 mm and 2.16 +/- 0.37 mm at the insertion into the pituitary gland, respectively, and are 3.25 +/- 0.43 mm and 3.35 +/- 0.44 mm at the level of the optic chiasm. The length of the infundibulum measures 5.91 +/- 1.24 mm, and the depth of the infundibular recess is 4.69 +/- 0.87 mm.[7] The signal intensity of the normal pituitary infundibulum on T1-weighted imaging should be slightly less than the optic chiasm and always less that the posterior pituitary gland. The pituitary infundibulum lacks a blood-brain barrier and, therefore, enhances intensely.

Idiopathic Central Diabetes Insipidus

Idiopathic central diabetes insipidus causes 12% to 50% of cases of central diabetes insipidus in children.[8,9] The majority of these patients will present with absence of the posterior pituitary bright spot on MR imaging. Patients may also have anterior pituitary hormone deficiencies. The pituitary infundibulum may be normal or thickened at presentation. On follow-up imaging, the infundibulum may change in thickness over time.[8,9] No focal-enhancing mass will be detected on imaging. As the name implies, the etiology of this condition remains unknown and this remains a diagnosis of exclusion.

Ectopic Posterior Pituitary Bright Spot

An ectopic posterior pituitary bright spot will have a characteristic appearance on MR imaging, as the bright spot will be within the infundibulum or hypothalamus instead of within the dorsal aspect of the sella (**Figure 4**). Early descriptions of an ectopic posterior pituitary gland proposed an underlying traumatic etiology. However, more recent studies have favored an underlying genetic basis for the disorder.[10,11] An ectopic posterior pituitary bright spot can be seen in patients with congenital pituitary hypoplasia and associated growth hormone deficiency. There may be associated hypoplasia or absence of the adenohypophysis and pituitary infundibulum. When the posterior pituitary bright spot is ectopic, there is a higher incidence of associated brain and skull-base anomalies as well as callosal anomalies. There are also associations with Chiari I malformation, septo-optic dysplasia, periventricular gray matter heterotopia, microcephaly, persistent cranio-pharyngeal canal, basilar impression, medial deviation of the carotid arteries, cerebellar atrophy, single central incisor tooth, vermian dysplasia, and Kallmann syndrome.[12]
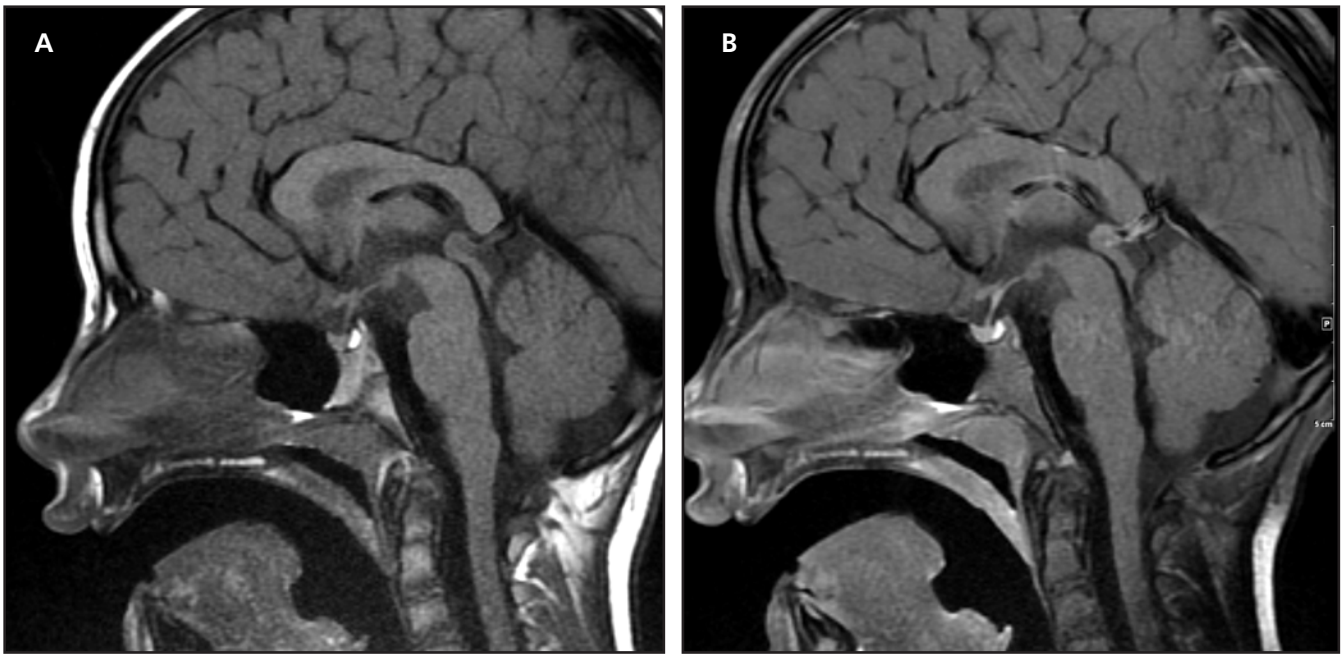
FIGURE 3. *Normal appearance of the pituitary gland in a 5-year-old child. Sagittal T1 (A) and sagittal T1 post contrast (B).*

FIGURE 4. *Ectopic posterior pituitary bright spot in a 7-year-old boy. Sagittal T1 (A) and sagittal T1 post contrast (B) demonstrate an ectopic posterior pituitary bright spot located along the superior aspect of the pituitary infundibulum.*

Germ Cell Tumors

Germ cell tumors include germinomas, nongerminomatous germ cell tumors, and teratomas. These most commonly present along the midline involving the pineal region (45%) and/or suprasellar region (30%).[1] Additional sites include the basal ganglia, cerebellopontine angle, cerebellum, and the spinal cord. These tumors may be mature or immature and can present with malignant degeneration. Suprasellar germ cell tumors originate within the infundibular recess of the hypothalamus. Infiltration of the infundibulum by the tumor will result in disruption of the axons that carry ADH from the paraventricular and supraoptic nuclei of the hypothalamus to the posterior pituitary gland.[1] This will result in diabetes insipidus characterized by excessive thirst, electrolyte imbalance, and frequent urination. The normal pituitary bright spot will be absent on MRI. An important note is that when children present with diabetes insipidus related to a germinoma, the only finding that may be present on the initial brain MRI is absence of

FIGURE 5. Germinoma in a 10-year-old boy. Sagittal T1 (A) and sagittal T1 post contrast (B) demonstrate an expansile and enhancing mass involving the pituitary infundibulum.

FIGURE 6. Langerhans cell histiocytosis in a 7-year-old boy. Sagittal T1 (A) and sagittal T1 post contrast (B) demonstrate an enhancing mass centered in the hypothalamus. Sagittal T1 (C) demonstrates severe height loss of the C5 vertebral body "vertebral plana."

FIGURE 7. Lymphocytic hypophysitis in an 11-year-old boy. Sagittal T1 (A) and sagittal T1 post contrast (B) demonstrate an expansile enhancing mass centered in the pituitary infundibulum.
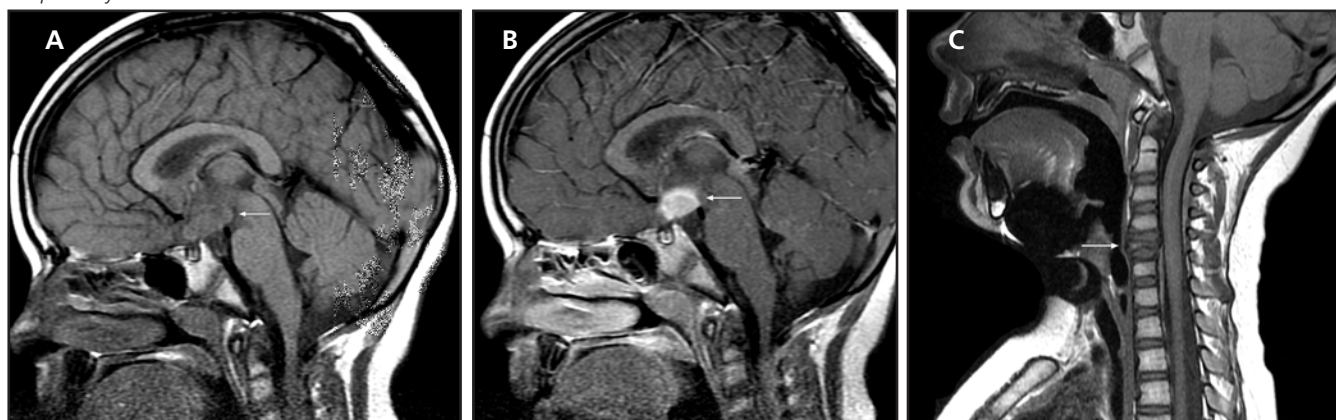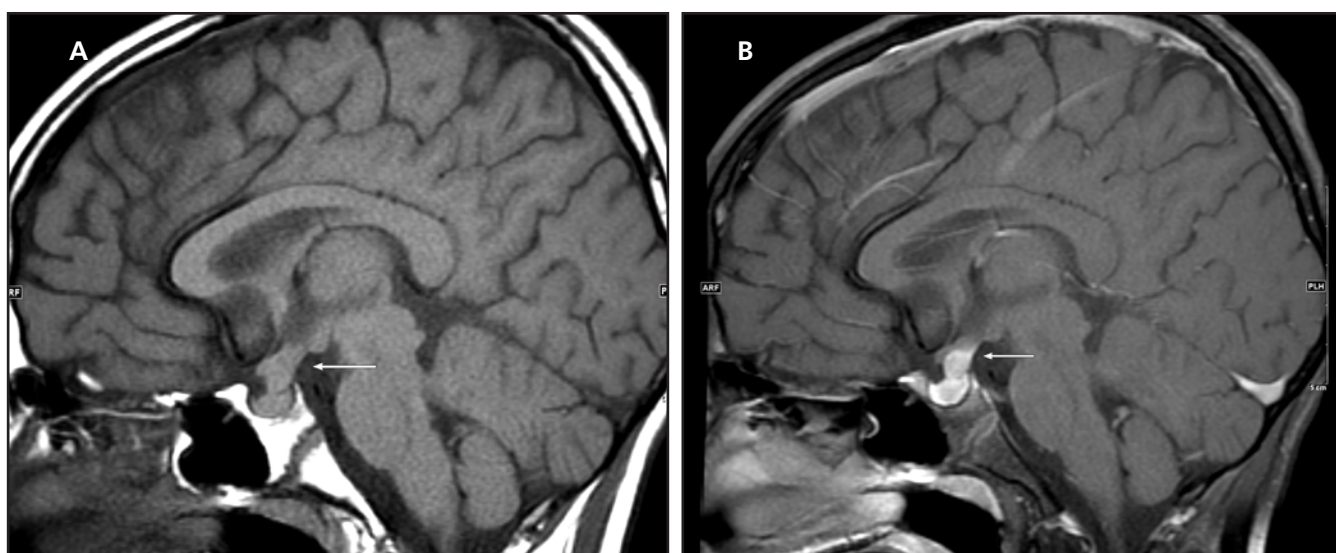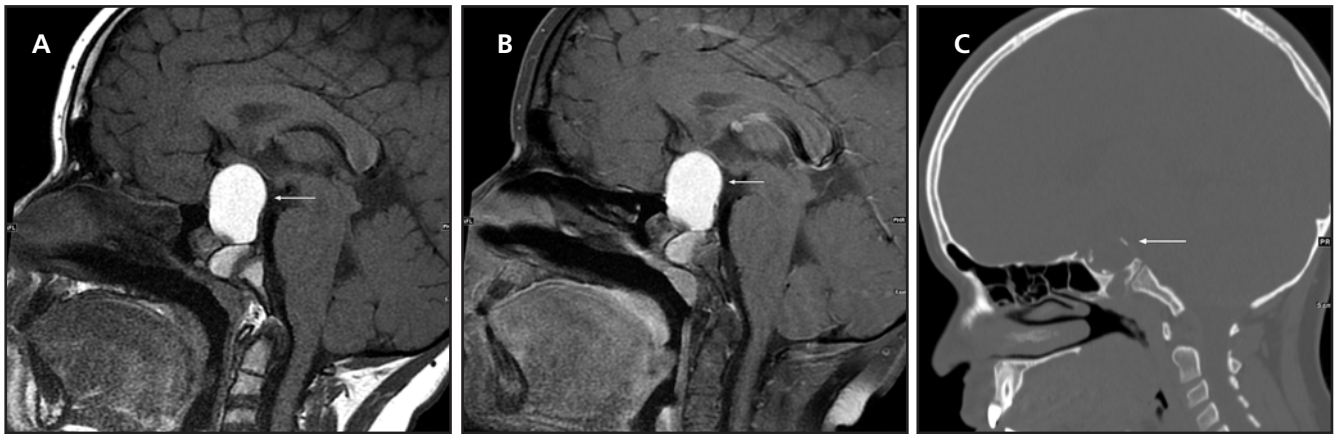
FIGURE 8. *Craniopharyingioma in a 10-year-old boy. Sagittal T1 (A) and sagittal T1 post contrast (B) demonstrate a large predominately intrinsically T1 hyperintense mass centered in the sella and suprasellar region. The is a small enhancing component of the mass within the sella. Sagittal CT reformat (C) demonstrates areas of calcification along the periphery of the mass.*
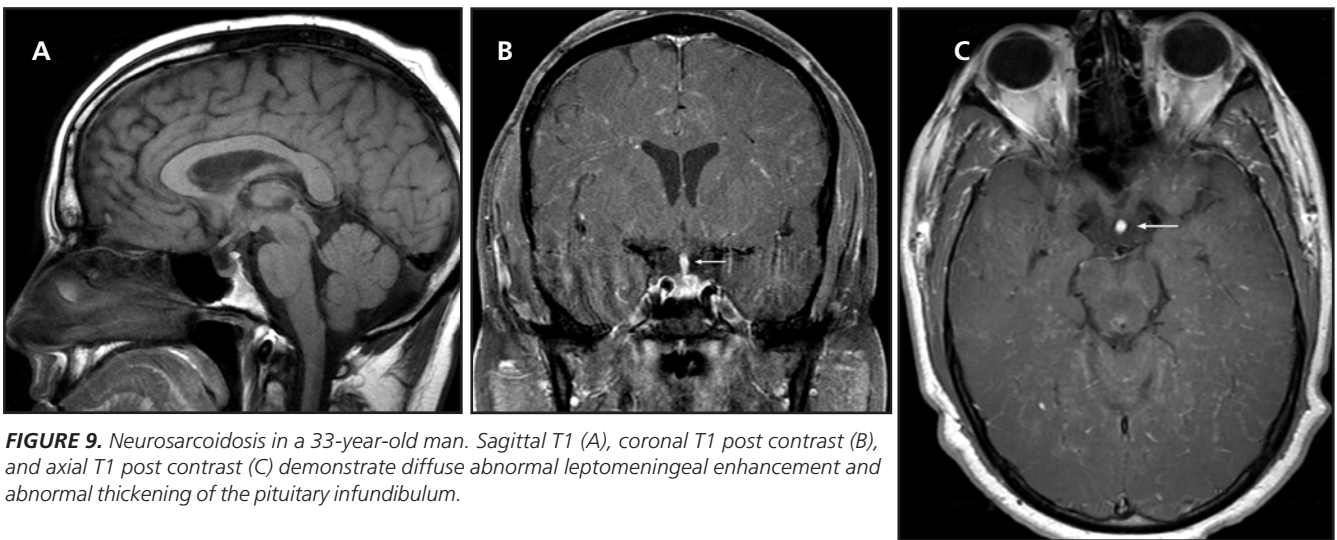

FIGURE 9. *Neurosarcoidosis in a 33-year-old man. Sagittal T1 (A), coronal T1 post contrast (B), and axial T1 post contrast (C) demonstrate diffuse abnormal leptomeningeal enhancement and abnormal thickening of the pituitary infundibulum.*

the normal posterior pituitary bright spot. This is related to the germinoma being exceedingly small and essentially undetectable by MRI. It is imperative to follow these children with serial MRIs, as the germinoma will grow over time and become detectable with imaging. Current thinking is to follow these children with serial MRIs for at least 3 years. If no abnormality develops on MRI after 3 years, the frequency of follow-up MRIs can be decreased.[9]

All histologic subtypes of germinomas are relatively hypercellular. Therefore, these tumors demonstrate high attenuation on CT and are isointense to gray matter on T1- and T2-weighted sequences. These tumors do not have a blood-brain barrier and will demonstrate avid postcontrast enhancement

(**Figure 5**). Following treatment of the germinoma, the absence of the posterior pituitary bright spot will last forever and clinical symptoms of diabetes insipidus will persist.[1]

Langerhans Cell Histiocytosis

Langerhans cell histiocytosis (LCH) is the most common histiocytic disorder of the central nervous system (CNS). LCH is a clonal proliferative disorder of cells of the mononuclear phagocytic and dendritic cell system of unknown pathophysiology and is considered a mix between immune dysregulation, inflammation, and malignancy. Classic pathologic findings include histiocytes with cleaved nuclei (coffee bean) that have CD1a and CD207 cell surface antigens in a background of plasma

cells, multinucleated giant cells, lymphocytes, and eosinophils.[13] Clinical presentations of LCH are variable and range from single-organ involvement to extensive multisystem involvement. Most frequently involved sites include bone, skin, spleen, liver, lymph nodes, and thymus. Calvarial and bone lesions will show preferential involvement of the outer table compared to the inner table, creating the characteristic "bone in bone" appearance. Near complete height loss of a vertebral body "vertebral plana" is often seen in the spine. When LCH involves the CNS, which occurs in 4% to 25% of patients, the most common location involved is the pituitary infundibulum.[13,14] Granulomas will develop within the pituitary infundibulum, hypothalamus, and adjacent
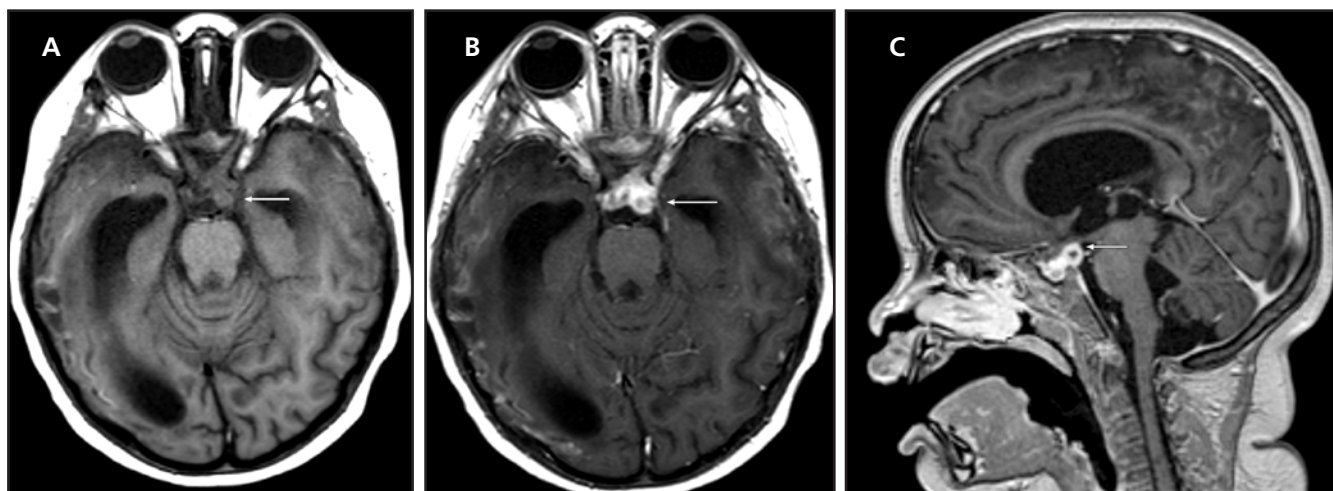
FIGURE 10. CNS tuberculosis in a 3-year-old girl. Axial T1 (A), Axial T1 post contrast (B), and sagittal T1 post contrast (C) demonstrate peripheral enhancing masses in the region of the sella and suprasellar cistern.

subarachnoid space. These granulomas will demonstrate avid postcontrast enhancement and result in expansion of the infundibulum and hypothalamus (**Figure 6**). Once approximately 80% of the axons carrying ADH within the infundibulum are disrupted, the clinical symptoms of diabetes insipidus will begin and the posterior pituitary bright spot will disappear.[1,15] In patients who present with multisystem involvement, the diagnosis may potentially be made from biopsy of enlarged lymph nodes or spine lesions rather than the pituitary infundibulum. Following treatment of LCH, the normal posterior pituitary bright spot will reappear and symptoms of diabetes insipidus should resolve.

Lymphocytic Hypophysitis

Lymphocytic hypophysitis is a neuroendocrine disorder characterized by autoimmune infiltration of the pituitary gland by lymphocytes and plasma cells. The disorder can be divided into two subtypes: adenohyphysitis (LAH), which involves the anterior pituitary gland, and infundibuloneurohypophysitis (LINH), which involves the posterior pituitary gland, infundibulum, and hypothalamus. LINH can occur in both adults and children and often will present clinically with acute onset of diabetes insipidus and headache. MR imaging will show enlargement of the infundibulum, hypothalamus, and

potentially the pituitary gland. Infiltration of the infundibulum will often result in absence of the normal posterior bright spot. The enlarged structures will demonstrate avid postcontrast enhancement (**Figure 7**). Imaging characteristics are often identical to suprasellar germinomas and LCH.[1,16]

Craniopharyingioma

Craniopharyngiomas account for 50% of suprasellar tumors in children.[1] The adamantinomatous type is the most common in children. These tumors most commonly arise from the tuber cinereum of the hypothalamus but can also arise from the pituitary gland, infundibulum, or infrasellar sphenoid bone. If the tumor disrupts the axons between the hypothalamus and posterior pituitary gland, there will be associated absence of the posterior pituitary bright spot. These tumors often contain cystic and solid components. The cystic components have variable T1 signal and hyperintense T2 signal. The solid tissue within the tumor will enhance and the cysts will demonstrate peripheral enhancement (**Figure 8**). Approximately 90% of craniopharyingiomas will contain a component of calcification. The calcification may be thin and along the margin of a cyst "eggshell" pattern or course within the solid portion of the mass. A mixed cystic and solid, partially calcified, enhancing mass in the

suprasellar region in a child is almost always a craniopharyngioma.[1,17]

Neurosarcoidosis

Sarcoidosis is an idiopathic systemic granulomatous disorder that results in the development of noncaseating granulomas in various organs. The etiology of sarcoidosis remains unknown. Studies have shown that both genetic and environmental factors may play a role in the development of the disease. Symptomatic CNS sarcoidosis is present in 5% to 15% of patients with sarcoidosis and most of these patients have extra neural manifestations of sarcoidosis. Isolated involvement of the CNS is rare, involving only 1% of all patients with sarcoidosis.[18,19] Sarcoidosis can involve the leptomeninges, dura, and brain parenchyma (**Figure 9**). Sarcoid granulomas can form anywhere within the brain parenchyma and are often found within the hypothalamus and pituitary infundibulum, which may result in diabetes insipidus. The parenchymal lesions will demonstrate hypointense T1 signal, hypointense T2 signal, and avid postcontrast enhancement. The definitive diagnosis of neurosarcoidosis requires biopsy; however, in many instances this may not be feasible. The probable diagnosis can be made with the confirmation of systemic sarcoidosis, CSF studies, and MRI features of neurosarcoidosis.

Tuberculosis

Meningitis is one of the most common extrapulmonary manifestations of infection by *Mycobacterium tuberculosis*. Tuberculomas, meningovasculitis, and miliary involvement of the CNS can all also occur in children with tuberculosis. Infiltration of the pituitary infundibulum by the thick exudate related to TB meningitis or development of a tuberculoma within the infundibulum can result in diabetes insipidus. Brain tuberculomas show different imaging features at each stage of evolution. These are divided into noncaseating tuberculomas, solid caseating tuberculomas, and tuberculomas with central liquefaction. Noncaseating tuberculomas are solid lesions without necrosis and demonstrate hypointense T1 signal, hyperintense T2 signal, and homogenous enhancement. Solid caseating tuberculomas have a central caseating zone of necrosis and demonstrate isointense to hypointense T1 signal, slightly T2 hypointense signal, and ring enhancement. The last stage of brain TB are tuberculomas with central liquefaction and have a similar appearance to other infectious intracranial abscesses. These abscesses will demonstrate central T1 hypointensity, central T2 hyperintensity, central diffusion restriction, and ring enhancement (**Figure 10**). Unlike bacterial abscesses, TB abscesses elicit little surrounding vasogenic edema. The diagnosis of CNS TB can often be made with CSF studies and MRI findings.[20,21]

Wolfram Syndrome

Wolfram syndrome is a rare autosomal recessive disorder (1 in 770,000) featuring diabetes insipidus, diabetes mellitus, optic atrophy, and deafness. The gene for Wolfram syndrome has been mapped to chromosome 4p, which is responsible for endoplasmic reticulum stress-mediated cell death. Typical MR brain findings include absence of the normal posterior pituitary bright spot, bilateral intraorbital and intracranial optic nerve atrophy, T2 hyperintense signal in the pons, and progressive brainstem and cerebellar atrophy. No current treatments are available for this disease and life expectancy is approximately 30 years.[22,23]

Conclusion

Central diabetes insipidus commonly will manifest on imaging with absence of the normal posterior pituitary bright spot; this absence in children is always abnormal. Idiopathic central diabetes insipidus is a diagnosis of exclusion. A normal brain MRI (except for absence of the posterior pituitary bright spot) in a child with central diabetes insipidus does not exclude a germinoma or LCH. The lesion may be undetectable at initial MRI, and follow-up imaging is critical. Lymphocytic hypophysitis can have identical imaging characteristics to germinoma and LCH but is more common in young adults than children. Craniopharyngiomas commonly have a combination of cysts, solid enhancing components, and calcifications, making them easier to diagnose with imaging alone. Isolated neurosarcoidosis is rare so the diagnosis can often be made with identification of lesions involving different parts of the body. Signs of systemic infection may be present in patients with CNS involvement with tuberculous, and CSF studies can be helpful.

References

1. Barkovich AJ, Raybaud C. Intracranial, Orbital, and Neck Masses. Pediatric Neuroimaging. 6th ed. Wolters Kluwer; 2019:758-782.
2. Fujisawa I, Asato R, Nishimura K, et al. Anterior and posterior lobes of the pituitary gland: assessment by 1.5 T MR imaging. J Comput Assist Tomogr 1987;11(2):214-220.
3. Hong GK, Payne SC, Jane JA Jr. Anatomy, physiology, and laboratory evaluation of the pituitary gland. Otolaryngol Clin North Am 2016;49(1):21-32.
4. Treschan TA, Peters J. The vasopressin system: physiology and clinical strategies. Anesthesiology 2006;105(3):599-640.
5. Côté M, Salzman KL, Sorour M, Couldwell WT. Normal dimensions of the posterior pituitary bright spot on magnetic resonance imaging. J Neurosurg 2014;120(2):357-362.
6. Brooks BS, el Gammal T, Allison JD, Hoffman WH. Frequency and variation of the posterior pituitary bright signal on MR images. Am J Neuroradiol 1989;10(5):943-948.
7. Satogami N, Miki Y, Koyama T, Kataoka M, Togashi K. Normal pituitary stalk: high-resolution MR imaging at 3T. Am J Neuroradiol 2010;31(2):355-359.
8. Maghnie M, Cosi G, Genovese E, et al. Central diabetes insipidus in children and young adults. N Engl J Med 2000;343(14):998-1007.
9. Werny D, Elfers C, Perez FA, Pihoker C, Roth CL. Pediatric central diabetes insipidus: brain malformations are common and few patients have idiopathic disease. J Clin Endocrinol Metab 2015;100(8):3074-3080.
10. Argyropoulou M, Perignon F, Brauner R, Brunelle F. Magnetic resonance imaging in the diagnosis of growth hormone deficiency. J Pediatr 1992;120(6):886-891.
11. Hamilton J, Blaser S, Daneman D. MR imaging in idiopathic growth hormone deficiency. Am J Neuroradiol 1998;19(9):1609-1615.
12. Mitchell LA, Thomas PQ, Zacharin MR, Scheffer IE. Ectopic posterior pituitary lobe and periventricular heterotopia: cerebral malformations with the same underlying mechanism? Am J Neuroradiol 2002;23(9):1475-1481.
13. Wang Y, Camelo-Piragua S, Abdullah A, Ibrahim M, Parmar HA. Neuroimaging features of CNS histiocytosis syndromes. Clin Imaging 2020;60(1):131-140.
14. Prayer D, Grois N, Prosch H, Gadner H, Barkovich AJ. MR imaging presentation of intracranial disease associated with Langerhans cell histiocytosis. Am J Neuroradiol 2004;25(5):880-891.
15. Maghnie M, Aricò M, Villa A, Genovese E, Beluffi G, Severi F. MR of the hypothalamic-pituitary axis in Langerhans cell histiocytosis. Am J Neuroradiol 1992;13(5):1365-1371.
16. Faje A. Hypophysitis: evaluation and management. Clin Diabetes Endocrinol 2016;2:15. doi:10.1186/s40842-016-0034-8
17. Lee IH, Zan E, Bell WR, Burger PC, Sung H, Yousem DM. Craniopharyngiomas: radiological differentiation of two types. J Korean Neurosurg Soc 2016;59(5):466-470.
18. Ganeshan D, Menias CO, Lubner MG, Pickhardt PJ, Sandrasegaran K, Bhalla S. Sarcoidosis from head to toe: what the radiologist needs to know. RadioGraphics 2018;38(4):1180-1200.
19. Baughman RP, Teirstein AS, Judson MA, et al. Clinical characteristics of patients in a case control study of sarcoidosis. Am J Respir Crit Care Med 2001;164(10 Pt 1):1885-1889.
20. Patankar T, Patkar D, Bunting T, Castillo M, Mukherji SK. Imaging in pituitary tuberculosis. Clin Imaging 2000;24(2):89-92.
21. Rodriguez-Takeuchi SY, Renjifo ME, Medina FJ. Extrapulmonary tuberculosis: pathophysiology and imaging findings. RadioGraphics 2019;39(7):2023-2037.
22. Ito S, Sakakibara R, Hattori T. Wolfram syndrome presenting marked brain MR imaging abnormalities with few neurologic abnormalities. Am J Neuroradiol 2007;28(2):305-306.
23. Gocmen R, Guler E. Teaching NeuroImages: MRI of brain findings of Wolfram (DIDMOAD) syndrome. Neurology 2014;83(24):e213-e214.

Cystic Lesion of the Mandibular Ramus

Farooq Choudhry, M.D.

Department of Radiological Sciences, University of Oklahoma College of Medicine, Oklahoma City, OK

Case Presentation

A 55-year-old woman presented with persistent right jaw pain for 2 months, with no history of a recent dental procedure and no symptoms to suggest infection. A pantomogram was obtained (**Figure 1**) followed by CT imaging (**Figure 2**).

Key Clinical Finding

Persistent jaw pain

Key Imaging Finding(s)

Expansile cystic/lytic bone lesion within the mandibular ramus without a soft-tissue component or enhancement

Differential Diagnosis

Keratocystic odontogenic tumor (OKC)
Dentigerous cyst
Ameloblastoma (unicystic form)
Benign fibro-osseous lesion (ossifying fibroma)

Discussion

Cystic lesions of the mandibular ramus may first be detected by radiographs and may require CT imaging for further evaluation. The initial presentation is variable with respect to pain. Given that a solid mass can produce lytic changes in bone, it is best to characterize a lesion as "lucent" on radiographs and defer any attempts to differentiate cystic lesions from solid lytic lesions until cross-sectional imaging is available. In this case, the mandibular lesion begins in the retromolar location and extends to the condyle. There is no enhancement, periosteal reaction, or involvement of surrounding musculature to suggest an aggressive malignant neoplasm. The presence of a thick sclerotic cortex suggests a more indolent process as the bone

FIGURE 1. Panorex shows an expansile lucent lesion involving the right mandibular ramus.

is attempting normal repair around the lesion. Fibrous dysplasia is not included in the differential considerations since there is no evident matrix within the lesion. Dentigerous cyst is considered unlikely since the closest molar tooth is not involved. The most likely consideration is keratocystic odontogenic tumor (OKC) vs unicystic ameloblastoma. Tissue sampling from the cyst wall can be obtained using CT guidance. Although these are benign lesions, they are locally aggressive and may recur.

Keratocystic Odontogenic Tumor

Keratocystic odontogenic tumor (OKC) is not currently classified as a tumor despite the moniker. An OKC is a benign periapical cyst of the mandible or maxilla that falls into the developmental lesion category of the 2017 World Health Organization classification of odontogenic and maxillofacial bone tumors.[1] Most cases are nonsyndromic but multiple lesions are a hallmark of Gorlin syndrome (Nevoid basal cell carcinoma syndrome) due to PTCH mutations. Additional syndromic associations of OKC include Noonan syndrome and Ehlers-Danlos syndrome. Multiple OKCs in these conditions are typically asynchronous, occurring over a lifetime.[2] OKCs are mostly seen

in younger patients in their teens, 20s or 30s, are locally aggressive and can recur after excision.[3] Many patients with keratocystic odontogenic tumors are asymptomatic, but some will present with jaw swelling and pain. The surgical path specimen will reveal a thin-walled cyst with fluid and debris, resulting in a variable consistency.[3] These tumors arise from stratified squamous keratinizing epithelium found along the margin of the dental lamina and the periodontal margin of the alveolus.[3] When these tumors arise from the mandible they typically arise from the posterior aspect of the mandible.[4] These lesions can arise near the roots of teeth similar to radicular cysts from dental caries or can arise near the crown of an unerupted/impacted tooth similar to a dentigerous cyst.[4] OKCs may be multilocular and daughter cysts can develop if perforation of the bony cortex occurs.

Dentigerous Cyst

Dentigerous cysts occur within the mandible or the maxilla, and when large can grow into the maxillary sinus or result in a pathologic fracture of the mandible. These lesions are not seen in childhood because they occur almost exclusively with secondary/permanent dentition, and often with unerupted/
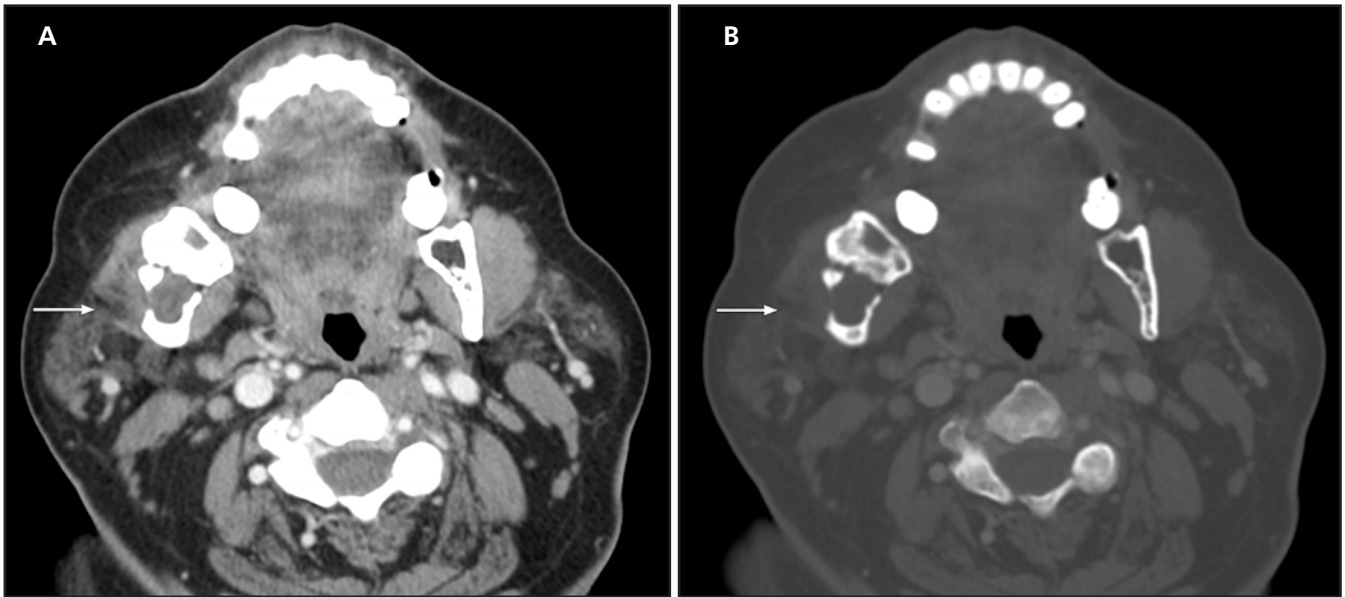
FIGURE 2. *Axial CT images obtained after intravenous administration of contrast are displayed in soft tissue (A) and bone windows (B). There is a nonenhancing, lytic, and expansile lesion involving the right mandibular ramus with areas of cortical thinning/dehiscence in addition to other areas of sclerotic thickened cortex. The lesion extends to the mandibular condyle resulting in subluxation of the temporomandibular joint.*

impacted teeth. For this reason, third molars are a common location.[3] These pericoronal cysts attach to the cementoenamel junction of the tooth. These cysts occur more frequently in Gorlin syndrome but are derived from nonkeratonizing epithelium in contrast with keratocystic odontogenic tumors. Pain is uncommon.[3]

Ameloblastoma

Ameloblastoma is a locally aggressive benign tumor associated with BRAF mutations located within the mandible or, less commonly, the maxilla. Patients are often in their 20s or 30s, similar to odontogenic keratocysts.[4] These tumors arise from the cells responsible for enamel production that form the crown of the tooth. Most conventional (multicystic) ameloblastomas have cystic and variably enhancing solid components with internal septae and present as firm, painless, expansile soap-bubble lesions often with tooth root resorption.[4] A unicystic form accounts for less than 15% of cases and can be indistinguishable from dentigerous cysts or odontogenic keratocysts by CT imaging if associated with the crown of an

uneruped/impacted tooth and lacking mural nodules or enhancement.[4] Another location where dentigerous cyst, odontogenic keratocyst, and unicystic ameloblastoma overlap is the premolar region of the maxillary alveolus where lesions often grow into the maxillary sinus. Treatment of an ameloblastoma with a nodule or solid component is similar to OKC and consists of en-bloc surgical resection. It should be noted that the term "adamantinoma" was historically used for ameloblastoma but is now discouraged since there is no histologic correlate between an ameloblastoma and the adamantinoma that occurs in long bones such as the tibia.

Benign Fibro-Osseous Lesion (Ossifying Fibroma)

This rare lesion is composed of fibrous tissue that may calcify over time, mostly in a peripheral distribution. The lesion may appear lucent or heterogeneously radiopaque. Most lesions will be small, and cortical breakthrough is uncommon.

Diagnosis

Ameloblastoma

Summary

When presented with a cystic-appearing lesion of the mandibular ramus without enhancement or mural nodule, considerations will include unicystic ameloblastoma, dentigerous cyst, and keratocystic odontogenic tumor. The unicystic form of ameloblastoma is less common than the multicystic form that has cystic and soft-tissue components. Dentigerous cyst is usually seen in the setting of an uneruped/impacted tooth, but OKC and ameloblastoma can also be seen with an uneruped/impacted tooth. Dental root resorption is more typical of an ameloblastoma and is uncommon for dentigerous cyst or OKC.

References

1. Wright JM, Vered M. Update from the 4th Edition of the World Health Organization Classification of Head and Neck Tumours: Odontogenic and Maxillofacial Bone Tumors. Head Neck Pathol 2017;11(1):68-77.
2. Marimuthu V, Shetty UA, Shetty P. Tetrad presentation of non-syndromic odontogenic keratocyst: an uphill diagnostic and therapeutic challenge. Dent Med Probl 2018;55(4):447-451.
3. Scholl R, Kellett H, Neumann D, Lurie A. Cysts and cystic lesions of the mandible: clinical and radiologic-histopathologic review. RadioGraphics 1999;19:1107-1124.
4. Devenney-Cakir B, Subramaniam RM, Reddy SM, Imsande H, Gohel A, Sakai O. Cystic and cystic-appearing lesions of the mandible: review. Am J Roentgenol 2011;196(6 Suppl):WS66-WS77.

Rare Developmental Brainstem Abnormality

Ali Ayub Khan, M.S.,[1] Khairuddin Memon, M.D.[2]

[1]University of Oklahoma College of Medicine, Tulsa, OK
[2]Department of Radiological Sciences, University of Oklahoma College of Medicine, Oklahoma City, OK

Case Presentation

A 5-month-old baby presented with congenital right facial palsy, bilateral hearing loss and feeding difficulties. The patient was born at 36 weeks' gestation by cesarean section with an uncomplicated delivery. The right facial weakness was present since birth. Genetic testing was negative. Additionally, echocardiogram and renal ultrasound were also normal. An electroencephalogram demonstrated epileptiform changes without seizures. Physical examination showed right facial weakness with response to touch bilaterally, diffuse increased motor tone in all extremities, and decreased truncal tone. No gross coordination abnormalities were seen. Subsequently, an MRI of the brain and internal auditory canals were performed (**Figures 1-4**).

Key Imaging Findings

Hypoplasia of the cerebellum and vermis
Hypoplasia of the middle cerebellar peduncles
Hypoplasia of the pons
Dorsal pontine bump
Absence of the 7th and 8th nerves

Differential Diagnosis

Joubert syndrome
Pontocerebellar hypoplasia
Pontine tegmental cap dysplasia

Discussion

Significant advancements in the prenatal and postnatal imaging techniques over recent years have improved our understanding of pediatric posterior fossa developmental abnormalities. Additionally, research in developmental biology and genetics have further helped in classification of congenital posterior fossa abnormalities. Congenital posterior fossa anomalies may be broadly divided into genetic malformations and anomalies due to disturbances during development such as infection and other processes.[1] The majority of the posterior fossa anomalies involve the cerebellum to some extent, resulting in hypoplasia or dysplasia. There are subtle differences between various posterior fossa anomalies and recognizing those differences on the initial imaging study is important in terms of identifying the correct diagnosis for patients and clinicians. Coronal T2, sagittal T1- and T2-weighted imaging, as well as balanced steady-state gradient echo sequences are helpful in diagnosing posterior fossa anomalies.

Joubert Syndrome

Joubert syndrome is an autosomal recessive disorder characterized by hypotonia, breathing abnormalities, and intellectual disabilities. The classic imaging appearance is the molar tooth sign consisting of thickened and horizontally oriented superior cerebellar peduncles, hypoplasia of the cerebellum and vermis, and a deep interpeduncular fossa.[2,3] In some variations of this syndrome, abnormalities also include dysmorphic appearance of the tectum and midbrain, hypoplasia of the pons, callosal dysgenesis, hippocampal malrotation, and migrational disorders.[3] This syndrome also may be associated with several systemic disorders including renal, ocular, hepatic, and skeletal abnormalities.

Pontocerebellar Hypoplasia

Pontocerebellar hypoplasia (PCH) is a group of autosomal recessive disorders characterized by hypoplasia of the cerebellum and pons.[4,5] The typical imaging findings include hypoplasia of the cerebellum including the cerebellar hemispheres with relative preservation of the vermis, resulting in a "dragonfly" appearance.[1] The normal pontine volume is significantly decreased. Delayed myelination may be present. The morphologic pattern of pontocerebellar hypoplasia, however, has also been shown in other etiologies such as extreme prematurity and neurometabolic diseases such as glycosylation type and patients with mutations in CASK
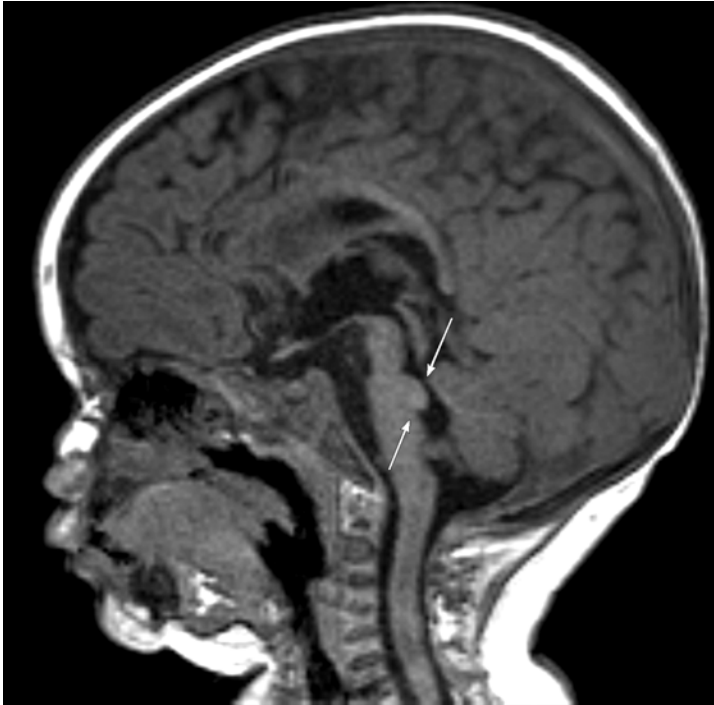
FIGURE 1. *Sagittal T1 image demonstrates flattening of the ventral pontine belly, and a prominent pontine tegmentum.*
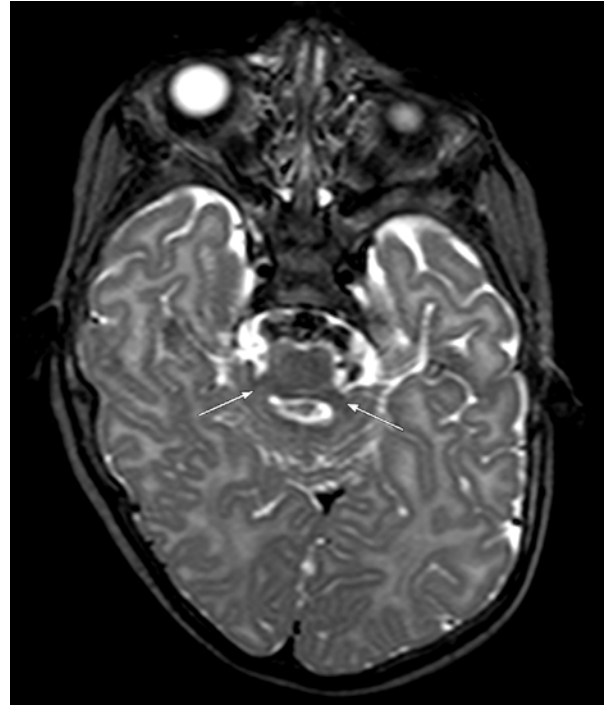

FIGURE 2. *Axial T2-weighted image demonstrates hypoplasia of the middle cerebellar peduncles.*

FIGURE 3. *Coronal T2-weighted image demonstrates vermian hypoplasia.*

FIGURE 4. *Axial FIESTA (balanced steady-state gradient echo sequence) image demonstrates absence of the bilateral 7th and 8th cranial nerves. (Images were previously published in an* American Journal of Neuroradiology Classic Case *on May 18, 2020.)*

(calcium/calmodulin-dependent serine protein kinase) gene. Morphologic pattern of pontocerebellar hypoplasia can also be seen with congenital muscular dystrophies that are caused by defective dystroglycan O-glycosylation.[6,7]

Pontine Tegmental Cap Dysplasia

Pontine tegmental cap dysplasia is a rare posterior fossa developmental abnormality with involvement of the vestibulocochlear, facial and trigeminal nerves, resulting in facial paralysis, and hearing loss among other abnormalities.[8] The characteristic imaging findings for this particular entity include a flattened appearance of the ventral pons (loss of the pontine belly) with a paradoxical bump involving the tegmentum of the pons, hypoplasia of the middle cerebellar peduncles, vermian hypoplasia, and absent inferior olivary prominence. This malformation is considered sporadic with an unknown genotype and the prognosis is highly variable. Diffusion tensor imaging may demonstrate absence of posterior positioning of the transverse pontine fibers. The underlying mechanism is uncertain but has been hypothesized to be related to abnormal migration of the neurons in the pontine tegmentum.[9]

Diagnosis

Pontine tegmental cap dysplasia

Conclusion

Malformations of the brainstem result in severe clinical manifestations, including feeding disorders, hearing loss, and cranial nerve palsies. Pontine tegmental cap dysplasia is a rather recently classified malformation. Helpful imaging findings in diagnosing this condition include volume loss of the normal pontine belly with a dorsal tegmental prominence, hypoplasia of the cerebellar vermis, hypoplasia of the middle cerebellar peduncles, and absence of the 7th and 8th cranial nerves. The disorder may be more common than previously thought and knowledge of its constellation of findings can aid accurate diagnosis.

References

1. Bosemani T, Orman G, Boltshauser E, et al. Congenital abnormalities of the posterior fossa. RadioGraphics 2015;35(1):200-220.
2. Gleeson JG, Keeler LC, Parisi MA, et al. Molar tooth sign of the midbrain-hindbrain junction: occurrence in multiple distinct syndromes. Am J Med Genet A 2004;125A(2):125-134; discussion 117.
3. Poretti A, Huisman TA, Scheer I, et al. Joubert syndrome and related disorders: spectrum of neuroimaging findings in 75 patients. Am J Neuroradiol 2011;32(8):1459-1463.
4. Barth PG. Pontocerebellar hypoplasias: an overview of a group of inherited neurodegenerative disorders with fetal onset. Brain Dev 1993;15(6):411-422.
5. Namavar Y, Barth PG, Kasher PR, et al. Clinical, neuroradiological and genetic findings in pontocerebellar hypoplasia. Brain 2011;134(pt 1):143-156.
6. Feraco P, Mirabelli-Badenier M, Severino M, et al. The shrunken, bright cerebellum: a characteristic MRI finding in congenital disorders of glycosylation type 1a. Am J Neuroradiol 2012;33(11):2062-2067.
7. Messerschmidt A, Brugger PC, Boltshauser E, et al. Disruption of cerebellar development: potential complication of extreme prematurity. Am J Neuroradiol 2005;26(7):1659-1667.
8. Barth PG, Majoie CB, Caan MW, et al. Pontine tegmental cap dysplasia: a novel brain malformation with a defect in axonal guidance. Brain 2007;130(pt 9):2258-2266.
9. Jissendi-Tchofo P, Doherty D, McGillivray G,. et al. Pontine tegmental cap dysplasia: MR imaging and diffusion tensor imaging features of impaired axonal navigation. Am J Neuroradiol 2009;30(1):113-119.

JAOCR at the Viewbox

Laith Alhyari, M.D., Benjamin O. Cornwell, D.O.

Department of Radiological Sciences, University of Oklahoma College of Medicine, Oklahoma City, OK
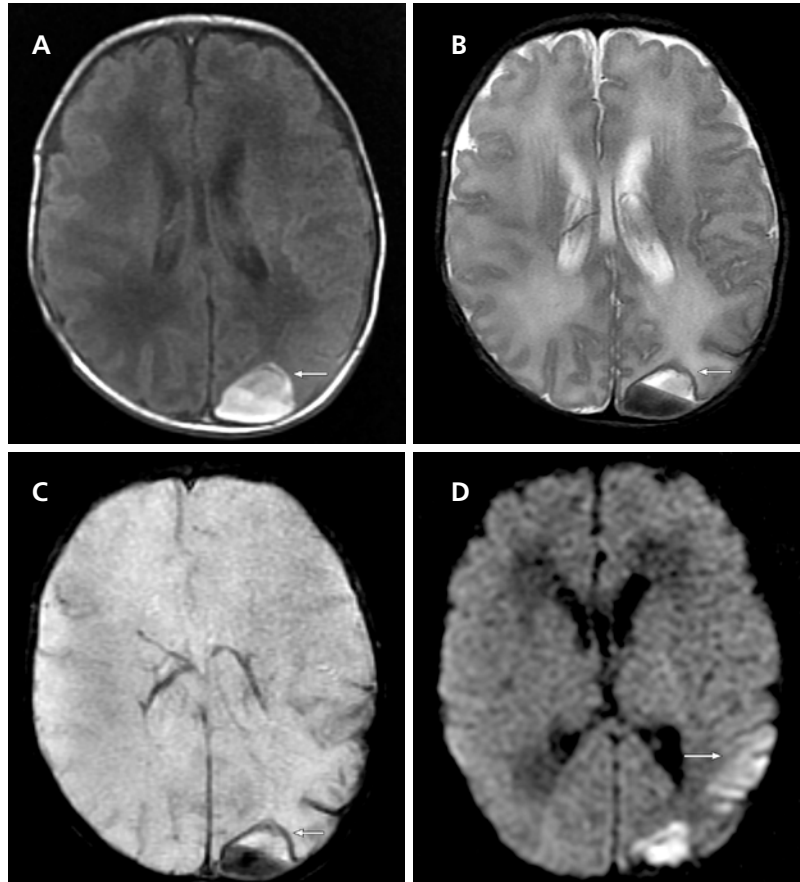
Subpial Hemorrhage in a Newborn

A term (37 weeks) newborn baby boy with suspicion for coarctation of the aorta on prenatal ultrasound had a head ultrasound performed to evaluate for structural anomalies. The head ultrasound revealed grade 1 germinal matrix hemorrhage and areas of hemorrhage in the left temporal/occipital region. A follow-up brain MRI revealed blood products expanding the subpial potential space with displacement of the adjacent sulci and extension along the calvarium over the left occipital lobe demonstrated on T1-weighted imaging (**A**), T2-weighted imaging (**B**), and gradient echo (**C**). There was an associated hematocrit level (**B, C**) within the hematoma. Diffusion-weighted imaging demonstrated cytotoxic edema in the adjacent left temporal lobe (**D**). The patient had no family history of bleeding disorders, prolonged umbilical bleeding, coagulation abnormalities, or birth trauma. The patient had an echocardiogram, which demonstrated a normal aortic arch without coarctation, which confirmed a false-positive prenatal ultrasound.

Subpial hemorrhage is a rare type of intracranial extra-axial hemorrhage with unclear mechanism and incidence.[1,2] It classically presents on imaging as hemorrhage, which courses along the surface of the brain but still has a confined appearance differentiating it from subarachnoid hemorrhage. Subpial hemorrhage is most common in the temporal lobes and close to suture lines.[1] Most cases demonstrate restricted diffusion within the adjacent brain parenchyma.[1]

Spontaneous subpial hemorrhage may occur in otherwise healthy term neonates but may also be related to birth trauma or coagulopathy.[2] The etiology remains unknown but may be related to thrombosis or compression of medullary veins along the surface of the brain.[1,2] Patients often present with apnea or seizures shortly after birth.[1]

REFERENCES

1. Huang AH, Robertson RL. Spontaneous superficial parenchymal and leptomeningeal hemorrhage in term neonates. Am J Neuroradiol 2004;25(3):469-475.
2. Cain DW, Dingman AL, Armstrong J, et al. Subpial hemorrhage of the neonate. Stroke 2020;51(1):315-318.

JAOCR at the Viewbox

Anjali Lai, M.D

Department of Radiological Sciences, University of Oklahoma College of Medicine, Oklahoma City, OK
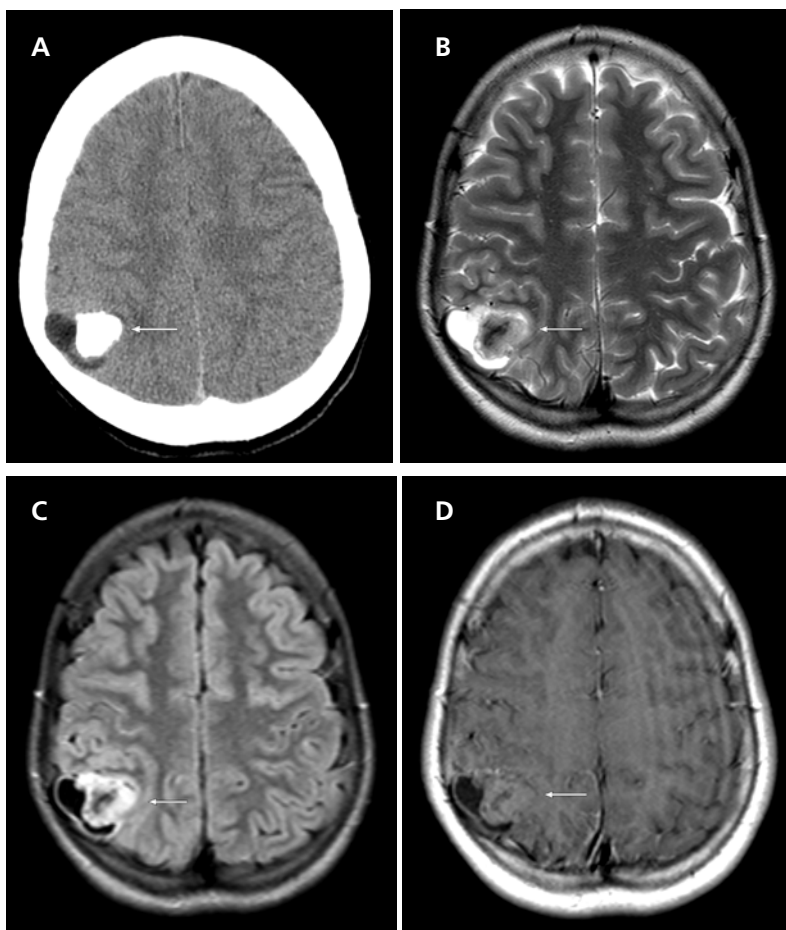
Polymorphous Low-Grade Neuroepithelial Tumor of the Young

A 12-year-old girl presented with new onset of seizures. The initial noncontrast head CT (**A**) demonstrated a right parietal mass with heavy calcification and cystic components. MRI revealed a well-defined mass with peripheral cysts demonstrating heterogenous signal on T2/FLAIR imaging (**B, C**) and no significant enhancement on postcontrast T1-weighted imaging (**D**). The lesion was resected and found to be a polymorphous low-grade neuroepithelial tumor of the young (PLNTY) on pathology.

First described in 2017, PLNTY is a rare tumor of the pediatric and young adult population. It is considered a subtype of low-grade neuroepithelial tumors that are typically associated with refractory epilepsy, such as gangliogliomas, dysembryoplastic neuroepithelial tumors (DNET), pleomorphic xanthoastrocytoma (PXA), and angiocentric gliomas. PLNTY usually occurs in the temporal lobe although instances have been reported within the parietal, frontal and occipital lobes.[1] On imaging, it is characteristically well-circumscribed with heterogenous signal on MR, macroscopic central calcification on CT, peripheral cystic components, and minimal to no enhancement.[2] PLNTY has not yet been classified by the World Health Organization, but clinically behaves like a WHO grade I tumor.[1]

References

1. Benson JC, Summerfield D, Carr C, et al. Polymorphous low-grade neuroepithelial tumor of the young as a partially calcified intra-axial mass in an adult. Am J Neuroradiol 2020;41(4):573–578.
2. Johnson DR, Giannini C, Jenkins RB, Kim DK, Kaufmann TJ. Plenty of calcification: imaging characterization of polymorphous low-grade neuroepithelial tumor of the young. Neuroradiology 2019;61(11):1327–1332.